Journal of Volcanology and Geothermal Research 282 (2014) 19–35

Contents lists available at ScienceDirect

Journal of Volcanology and Geothermal Research

journal homepage: www.elsevier.com/locate/jvolgeores

Evolution of a dynamic paleo-hydrothermal system at Mangatete, Taupo Volcanic Zone, New Zealand

Bryan D. Drake [a], Kathleen A. Campbell [a,*], Julie V. Rowland [a], Diego M. Guido [b], Patrick R.L. Browne [c], Andrew Rae [d]

[a] Geology, School of Environment, University of Auckland, Private Bag 92019, Auckland 1142, New Zealand
[b] CONICET and Facultad de Ciencias Naturales y Museo, Universidad Nacional de La Plata, Instituto de Recursos Minerales (INREMI), Calle 64 y 120, La Plata (1900), Argentina
[c] Institute of Earth Science and Engineering, University of Auckland, Private Bag 92019, Auckland 1142, New Zealand
[d] GNS Science, Wairakei Research Centre, Private Bag 2000, Taupo 3352, New Zealand

ARTICLE INFO

Article history:
Received 6 February 2014
Accepted 7 June 2014
Available online 21 June 2014

Keywords:
Taupo Volcanic Zone
New Zealand
Hot-spring deposit
Siliceous sinter
Hydrothermal eruption breccia
Silica residue
Faults

ABSTRACT

Recent quarrying and active faulting at Mangatete, Taupo Volcanic Zone (TVZ), New Zealand, illuminate a rare spatial and temporal window on a dynamic Late Quaternary geothermal system. Detailed geological mapping, stratigraphic logging, AMS ^{14}C dating, and textural and mineralogical analyses were used to construct a complex history of hydrothermal, volcanological and tectonic activity from ~36 to 2 ka. Extinct, surface hydrothermal manifestations occur over a ~2 km^2 area, and include *in situ* siliceous sinters distributed on normal fault terraces, an inferred hydrothermal eruption breccia (HEB) containing acid-etched sinter blocks, another probable HEB that was bathed in silicifying thermal fluids, and sinter clasts that were entrained in a debris flow associated with a volcanic ash event. Preserved sinter textures typical of near-neutral pH, alkali chloride spring discharge channels, aprons, terraces and affiliated marshes comprise plant-rich, palisade, tufted bubble mat, and domal stromatolitic fabrics. In addition, a packed fragmental sinter facies is shown herein to constitute silicified microbial mats that were broken, transported and deposited as point bar deposits in thermal spring-fed streams. Moreover, four unusual siliceous sinter fabrics—vuggy, globular spongy, scalloped, and arcuate wavy layered—are interpreted to have formed from local acid-sulfate-chloride thermal springs, possibly associated with paleo-fumaroles. The reconstructed history of paleo-hydrothermal activity indicates that the oldest sinters (~36 ka) at Mangatete developed in alkali chloride hot springs, but then underwent post-depositional alterion/overprinting by acid-sulfate steam condensate and were dismembered, possibly by a hydrothermal eruption. Low pH hot-spring discharges forming the unusual, inferred acid sinter fabrics were localized in the same area. A shift in paleo-hydrology is evidenced by unaltered, alkali chloride sinters dated between ~22 and 3 ka. A cluster of sinter dates between 22.7 and 20.7 ka denote thermal fluid emissions around the time of the Okareka eruption (~22.1 ka). An ~11 kyr gap in sinter ages followed, which overlaps with a time of relative quiescence in local fault movement in between the Rotorua and Rotoma eruptions, as determined from previous paleo-seismicity studies on the Whirinaki Fault in the Mangatete area. At ~9.4 ka, hot spring activity in thermally fed streams slightly post-dated the Rotoma eruption (~9.5 ka). The locations and ages of the youngest (post-9.4 ka) alkali chloride sinters and silicified paleosols in relation to Whirinaki Fault movements indicate an overall westward migration of siliceous spring discharge. Dated charcoal (~1.8 kyr) in ash at the base of a locally extensive, volcaniclastic debris flow, containing sinter blocks of a range of ages and mineralogical maturity, suggests its affiliation with the Taupo eruption. Mangatete sinters occur along SW–NE striking faults parallel to the regional trend of the TVZ, which dissect the topography into stepped terraces. Inferred basement cross-faults in the study area, i.e. structural lineaments orthogonal to this trend, may have served as fluid pathways at depth, initiating and maintaining hydrothermal activity at Mangatete for more than 30 kyr. Within the larger Ngakuru Graben (~150 km^2), the ages and distributions of sinters and hydrothermal eruption breccias, including those at Mangatete, show that significant hydrothermal activity occurred for more than 60 kyr, in an area lacking such activity today. Thus, Mangatete retains a rare stratigraphic record within the TVZ sinter archive of changing geothermal fluids, resulting from shifts in paleo-phreatic water levels. Moreover, although limited, the presented age data imply a relationship among seismic activity, volcanic ash fall events, and the occurrence of permeable pathways for upward migration of thermal fluids. Finally, whereas currently active TVZ geothermal fields appear to be stable over

* Corresponding author. Tel.: +64 9 3737599.
E-mail address: ka.campbell@auckland.ac.nz (K.A. Campbell).

http://dx.doi.org/10.1016/j.jvolgeores.2014.06.010

tens of thousands of years or more, the fossil hydrothermal systems in the wider Mangatete area demonstrate the possibility of much greater temporal variability in the lateral expression of local surface manifestations of thermal fluid discharge through time.

1. Introduction

Active high-temperature geothermal systems in continental settings result from large-scale, coupled transfer of heat and mass within the shallow crust, and can manifest subaerially as diverse hot springs and vapor discharges. Such systems indicate potential energy resources at depth (Lynne, 2012), and can have a close spatial relationship with epithermal mineralization (e.g., Fournier and Rowe, 1965; Krupp and Seward, 1987; Sillitoe, 1993; Guido and Campbell, 2011). Moreover, their surface manifestations serve as analog "extreme environments" for settings where life may have taken hold on early Earth and possibly other planets (e.g., Farmer and Des Marais, 1999; Farmer, 2000; Konhauser et al., 2003; Ruff et al., 2011). Fossil geothermal systems also provide evidence for the locations of past magmatism and thermal fluid flow in zones of crustal weakness. In this paper, we ascertain the changing paleo-hydrology of a well-exposed fossil geothermal system, the Mangatete sinter and associated deposits, Taupo Volcanic Zone (TVZ), New Zealand, which is preserved in an area that is today regarded as hydrothermally extinct. Our results provide new insights on the time-scales and variable fluid histories of the local surface manifestations of hydrothermal convection systems.

More than 20 major, active, high-temperature (>250 °C) geothermal systems occur within the TVZ (Fig. 1), an 18,000 km^2 region of active crustal extension (~10 mm/yr; e.g., Villamor and Berryman, 2001), typified by largely rhyolitic volcanism, and present-day high crustal heat flow (2600 MW/100 km) along the length of the rift axis (Bibby et al., 1995; Hochstein, 1995). High-temperature geothermal systems are recharged by meteoric water descending to depths of 7–8 km, where they are heated and rise to sustain large-scale hydrothermal convection plumes (Giggenbach, 1984; Hedenquist, 1986; Rowland and Sibson, 2004). The shallow boundaries of the geothermal systems are approximated by domains of low resistivity marking rising thermal fluids (Bibby et al., 1995). These fluids migrate through pre-volcanic basement in the TVZ to reach laterally extensive, near flat-lying, permeable, Quaternary volcaniclastic deposits (<1.6 Ma; Wilson et al., 1995), with local thicknesses of up to 3 km (e.g., Ngatamariki geothermal field; Boseley et al., 2010). The surface expression of a geothermal system can be offset laterally from its upflow by several kilometers (Hedenquist, 1986; Bertrand et al., 2012).

Most geothermal fluids may be categorized by three end-member, major anion-based compositions (Jones and Renaut, 2003; Renaut and Jones, 2011). First, bicarbonate springs generally produce travertine ($CaCO_3$) deposits, which result from dissolution of ascending CO_2 into shallow groundwater that later degasses, although travertine deposition also may be influenced by cyanobacteria (Farmer, 2000; Pentecost, 2003). Second, alkali chloride springs of nearly neutral pH originate from magmatically heated, deep reservoir-derived chloride waters saturated with amorphous silica, and typically form siliceous sinter (opal-A: $SiO_2.nH_2O$) deposits (White et al., 1956, 1964). Third, acid-sulfate waters develop where ascending H_2S oxidizes above the piezometric surface to cause dissolution of country rock, with some local precipitation of vapor phase (e.g., sulfur) and hydrothermal alteration minerals (e.g., kaolin, alunite and silica residue; Rodgers et al., 2004; Jones and Renaut, 2012). Where acid-sulfate waters mix with deep reservoir-derived chloride fluids (Ellis and Wilson, 1961; Krupp and Seward, 1987; Hedenquist and Browne, 1989), acid sinters may form (Jones et al., 1999a,b; 2000; Mountain et al., 2003; Schinteie et al., 2007). Such deposits are termed acid sinters because the silica originates from the deep, hot (>250 °C), chloride fluid reservoir, rather than leaching from surface country rock to form silica residue (Rodgers et al., 2002, 2004). Alkali chloride sinters and acid sinters are distinguished from one another based on differences in deposit thicknesses and textures, the latter of which are at least partly controlled by particular biotic compositions. In particular, near-neutral pH, alkali chloride springs deposit sinter of up to tens of meters in thickness, and sustain distinctive organism communities distributed over a temperature gradient (100 °C to ambient) from vent to distal apron

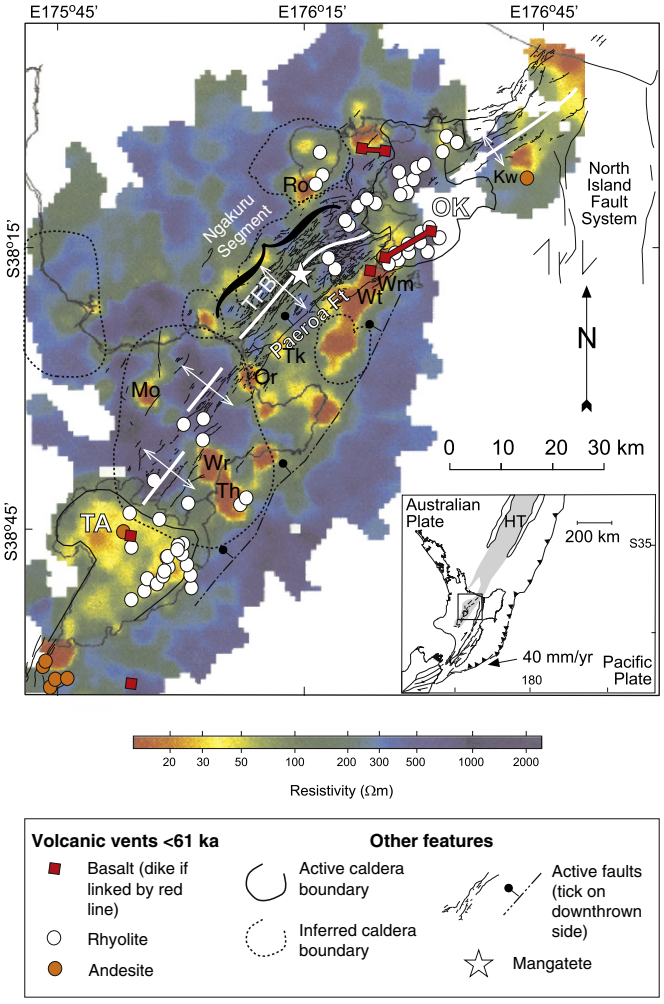

Fig. 1. Electrical resistivity map of the Taupo Volcanic Zone (TVZ), with nominal array spacing at 500 m (after Stagpoole and Bibby, 1998) in relation to rift segments, accommodation zones, interpreted basement structures (after Wan and Hedenquist, 1981; Rowland and Sibson, 2004), and inferred and active caldera boundaries (TA, Taupo; OK, Okataina; after Nairn, 2002). TFB = Taupo Fault Belt. Geothermal fields, indicated by low resistivity (color-coded red), are labeled as: Kw, Kawerau; Mo, Mokai; Or, Orakeikorako; Ro, Rotorua; Th, Tauhara; Tk, Te Kopia; Wm, Waimangu; Wr, Wairakei. Igneous composition of young (<61 kyr old) volcanic vents includes basalt (red squares), rhyolite (white circles), and andesite (orange circles). Rift axes are defined by changes in polarity of fault-facing directions, shown by white lines and annotated with extension direction as delineated by the pattern of active fault traces (Rowland and Sibson, 2001). The Mangatete study area (star) is situated in the Ngakuru tectonic segment. Inset shows submarine extension of the TVZ into the Havre Trough (HT), and position of the back arc rift system of the TVZ in relation to the active subduction margin of eastern North Island, New Zealand.

discharge areas (e.g., Walter, 1976; Cady and Farmer, 1996; Jones et al., 1997, 1998; Lowe et al., 2001; Handley and Campbell, 2011; Renaut and Jones, 2011; Lynne, 2012). In particular, non-photosynthetic microbial biofilms (Bacteria, Archaea) occur in very high temperature (>73 °C) vent pools and geyser mounds (Blank et al., 2002; Lowe and Braunstein, 2003). Luxuriant, colorful mats of photosynthetic bacteria readily silicify an array of fabrics within relatively high to moderate temperature (~65–40 °C), mid-apron terrace pools and outflow channels (Walter, 1976; Walter et al., 1976; Cady and Farmer, 1996). Clotted, encrusting and vertically pillared (palisade) microbial growths, entombed plants and various eukaryotes flourish in warm (~40–30 °C) to ambient temperatures on distal sinter apron terraces, as well as in adjacent, thermally influenced wetlands (e.g., Walter, 1976; Cady and Farmer, 1996; Farmer, 2000; Channing et al., 2004; Channing and Edwards, 2009; Guido and Campbell, 2011; Handley and Campbell, 2011). In contrast, low pH-tolerant algae (members of Cyanidiophyceae), fungi and diatoms are common biotic constituents in acid-sulfate geothermal areas today, and may become entombed in relatively thin (centimeters to ~decimeters thickness) acid sinter deposits occurring as sheets, ledges, ramparts, oncoids or spicules that reflect low silica accumulation rates and local environmental variability associated with mixed acid-sulfate-chloride springs (e.g., Jones et al., 1999a,b; Mountain et al., 2003; Schinteie et al., 2007; Jones and Renaut, 2012). Jarosite and clays also may be affiliated with acid sinter deposits (Jones et al., 1999a,b; Jones and Renaut, 2012). Thus, the biota, textures and mineralogy preserved in hot spring sinters may archive a record of shifting (paleo)temperature, (paleo)hydrodynamics and (paleo)fluid composition for a given site (Cady and Farmer, 1996; Jones and Renaut, 2007, 2012; Guido and Campbell, 2011; Handley and Campbell, 2011; Tewari and Seckbach, 2011; Tice et al., 2011; Jones and Renaut, 2012; Lynne, 2012).

Siliceous sinter facies and silica diagenesis have been investigated extensively in both active and fossil alkali chloride geothermal systems (e.g., Walter, 1976; Walter et al., 1976; Walter et al., 1996; Campbell et al., 2001; Jones et al., 2001, 2003; Guidry and Chafetz, 2003a,b; Lowe and Braunstein, 2003; Lynne and Campbell, 2003, 2004; Trewin et al., 2003; Rodgers et al., 2004; Lynne et al., 2005, 2006, 2007; Campbell and Lynne, 2006; Jones and Renaut, 2007; Guido and Campbell, 2011; Lynne, 2012). In comparison, less attention has been paid to: (1) facies signatures of mixed acid-sulfate-chloride springs; (2) the effects of falling ground water levels and subsequent alteration of sinter deposits by acid steam condensate; and (3) the complex interplay of changing spatial and temporal conditions in the shallow subsurface that place alkali chloride springs in close juxtaposition with acid springs in many geothermal areas (Jones et al., 1999a, 2000; Mountain et al., 2003; Rodgers et al., 2004; Campbell and Lynne, 2006; Lynne et al., 2006; Schinteie et al., 2007; Jones and Renaut, 2012; Rowland and Simmons, 2012; Murphy, 2013). Results of this study indicate that the Mangatete site preserves evidence of the former presence of alkali chloride and acid-sulfate-chloride fluids manifest in surface geothermal paleoenvironments, as detailed further below.

Within the TVZ, the Mangatete area of the Ngakuru tectonic segment (Figs. 1–5) constitutes an unusually well-exposed fossil hydrothermal system, where active normal faulting and quarrying for zeolites in underlying lacustrine tuffs (Brathwaite, 2003) have exposed a record of sinter deposition, paleosol formation, acid alteration, fault movement, and hydrothermal eruptions over ~30 kyr. In this study, the broad evolution of the paleo-geothermal field was determined *via* mapping of sinters, breccias, volcaniclastic deposits, and faults. Mineralogical and textural observations (Figs. 6–9) revealed paleoenvironmental and diagenetic signatures within the Mangatete sinters. Sinter and charcoal dates (Table 1) were integrated with respect to previously determined fault rupture events, calibrated with tephra dates, to reconstruct the relative timing of paleo-seismic, volcanic, and paleo-hydrologic events for the Mangatete area (Fig. 10). The Mangatete hydrothermal system also was evaluated in relation to past hydrothermal activity within the greater Ngakuru Graben area.

2. Geological context

2.1. Regional geology

The "young" TVZ (<340 ka) comprises a magmatically and structurally segmented rift system driven by subduction of the Pacific Plate beneath North Island (Australian Plate), which was initiated ~2 Ma atop Mesozoic metasedimentary basement rocks (Fig. 1; Wilson et al., 1995; Rowland and Sibson, 2001). Cone-building eruptions of andesite occur to the north and south of a central rhyolitic segment (Fig. 1) that is affected by explosive eruptions infilling calderas and rift basins with more than 15,000 km^3 of air-fall deposits, ignimbrites and lavas (Houghton et al., 1995; Wilson et al., 1995). The central segment also hosts rhyolitic dome complexes resulting from effusive volcanism. Basalts are rare at the surface (<1% total volume of exposed volcanic rocks) and in the explored subsurface, but may contribute to the enormous natural heat flow through the central TVZ (Bibby et al., 1995; Hochstein, 1995; Wilson et al., 1995). About 10 mm/yr of NW–SE extension across the central TVZ (Darby and Meertens, 1995; Wallace et al., 2004) is accommodated by ~20-km-long arrays of sub-parallel normal faults, vertical extension fractures and dike intrusions (Rowland and Sibson, 2001; Seebeck and Nicol, 2009; Rowland et al., 2010). Seismicity is dominated by widespread swarm activity with occasional moderate to large earthquakes (ML < 6.5; Bryan et al., 1999) defining a seismogenic zone 6 to 8 km deep that is presumably commensurate with maximum depths of the convecting hydrothermal fluids (Bibby et al., 1995).

Resistivity surveys mark the locations and dimensions of the active geothermal systems (Stagpoole and Bibby, 1998). Fig. 1 illustrates the spatial relationships among the geophysically delineated geothermal systems, accommodation zones, and rift segments. The geothermal fields occur in two SW–NE oriented, elongate zones of low resistivity that extend from the Taupo caldera to the Okataina volcanic center, parallel to the tectonic grain of the TVZ and separated from one another by the Taupo Fault Belt (Rowland and Sibson, 2004). The mean spacing between fields is 10–15 km. Several inferred basement structures trend perpendicular to the rift axis, coinciding spatially with transfer zones between adjacent rift segments and inferred NW-striking structures in the underlying graywackes (Wan and Hedenquist, 1981; Rowland and Sibson, 2004).

The Taupo Fault Belt (TFB, Fig. 1) is notably devoid of present day geothermal activity, although fossilized and relatively young sinters testify to activity in the recent past. For example, the Mangatete paleo-geothermal field (~2 km^2) occurs in the Ngakuru Graben (~150 km^2; Grindley, 1959), a ~9-km-wide subsiding basin of Quaternary pumice terraces and stratified lake sediments, situated between the Paeroa Fault to the east, and the Ngakuru Fault to the west (Fig. 2). The densely faulted axial zone of the Ngakuru tectonic segment (Fig. 1) is one of several rift sections that accommodate extension within the TVZ. Detailed mapping within the Ngakuru Graben (Rowland and Sibson, 2001; Villamor and Berryman, 2001; Canora-Catalán et al., 2008) has delineated a complex fault system of 10–15 parallel, SW–NE trending structural features, dipping both NW and SE and, in places, with parallel fault strands only 400 m apart. Fault trace-lengths vary from a few hundred meters to tens of kilometers, with splays making it difficult to distinguish separate faults. No NNW-striking faults were mapped by Villamor and Berryman (2001); whereas, we recorded NW–SE lineaments within the study area (Figs. 2 and 3), consistent with other reported NNW-oriented structures of the TVZ described in Rowland et al. (2010) and Downs et al. (2014a,b). Furthermore, Grindley (1959) mapped a ~1.5-km-gap in the Tahorakuri Formation (formerly known as the Ohakuri Formation; Gravley et al., 2006) horst at the location of the Mangatete quarries (Fig. 2), which suggests that a major NW–SE trending structure may be present at depth. Within the TFB, inferred

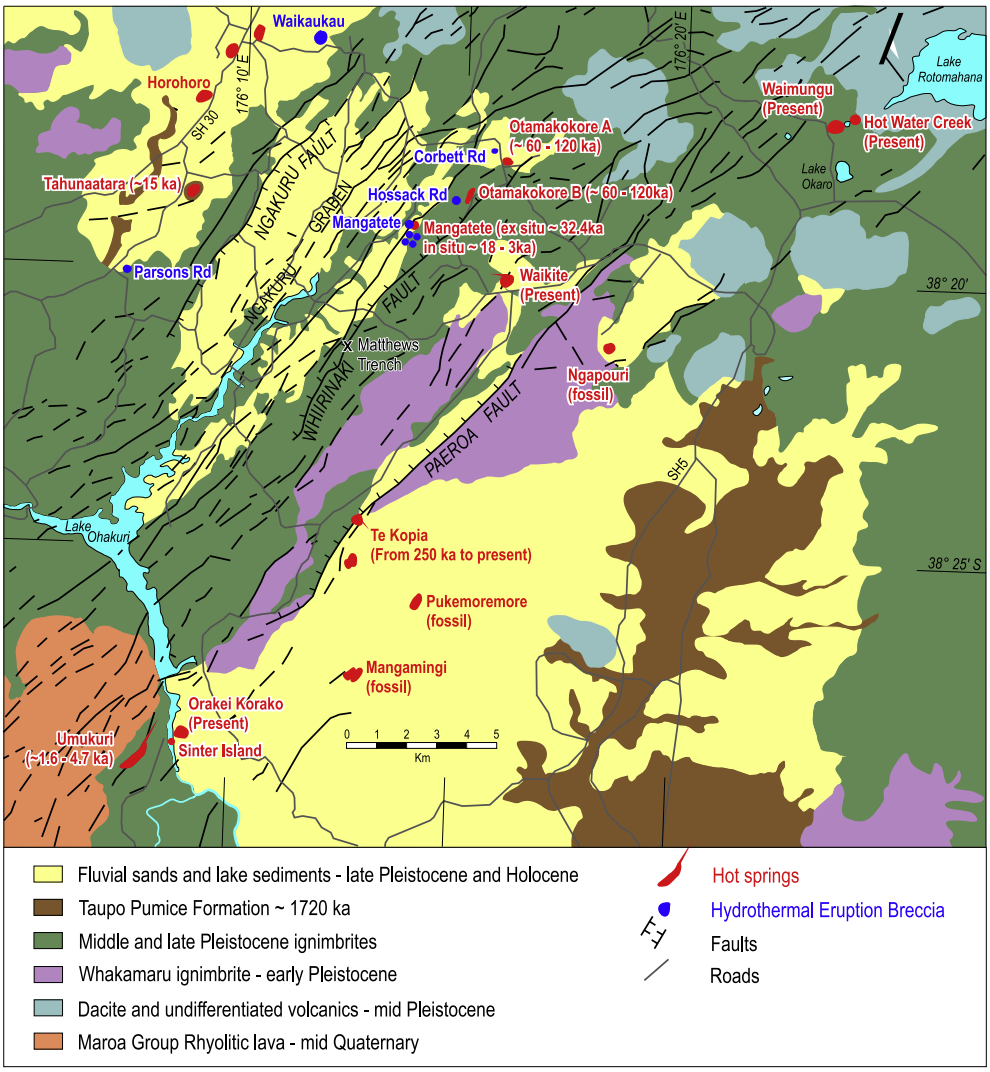

Fig. 2. Regional geology of Lake Rotomahana to Orakei Korako (after Leonard et al., 2010) showing location of the Mangatete study area within the Ngakuru Segment (graben), and geographic distribution of modern and fossil hydrothermal activity. Red areas indicate sinters; dark blue areas demarcate hydrothermal eruption breccias. Sites of (paleo)hydrothermal activity shown in the figure are discussed in detail in the text. Data for this figure were compiled from Wilson et al. (1995), Villamor and Berryman (2001), Brathwaite (2003), Campbell et al., 2004; Kissling and Weir (2005), Canora-Catalán et al. (2008), Rowland et al. (2010), Holland (2000), and from unpublished data.

cross-faults likely enhance permeability, allowing descending cold meteoric waters to recharge the paleo-hydrothermal convection system (cf. Bibby et al., 1995; Rowland and Sibson, 2004; Kissling and Weir, 2005; Dempsey et al., 2011). At Mangatete and within the Ngakuru Graben, such inferred cross-faults appear to have been locations of enhanced permeability, encouraging upward fluid flow and localized hydrothermal activity. Cross-faults are associated with hydrothermal activity elsewhere, including at Te Kopia on the Paeroa Fault (Fig. 2; Bignall and Browne, 1994), and affiliated with Jurassic epithermal mineralization sites of economic significance in Argentinean Patagonia (Guido and Campbell, 2011).

Extensive Quaternary lakes within the TVZ formed within calderas, becoming catchments for volcanic-derived sediments (Manville, 2001). They occur throughout the Ngakuru Graben as lacustrine volcaniclastic sandstones, siltstones and diatomite beds which are horizontal to sub-horizontal, thinly stratified, and poorly to moderately indurated (Villamor and Berryman, 2001; Brathwaite, 2003). Lake sediments of Late Pleistocene age at Mangatete, zeolitized by conductively heated groundwater (Brathwaite, 2003), are paraconformable with the overlying paleo-hydrothermal system described herein, which includes sinters, breccias and debris flow deposits (Figs. 3–5).

2.2. Mangatete study area

The Mangatete study site is located approximately 20 km south of Rotorua (Fig. 1), within the axial zone of the Ngakuru Graben (Fig. 2). Here, sinter and commercially valuable aggregates and zeolitized lake sediments are exposed in a 25-m-high scarp, the western strand of the Whirinaki Fault, including two small quarries that have been excavated into the footwall of this structure (Figs. 3–5). Thus, the Mangatete area hosts unusually good exposures of the local stratigraphy, including evidence of paleo-hydrothermal activity, volcanic ash fall events, and paleo-seismicity, discussed below.

The 21-km-long and up to 2-km-wide Whirinaki Fault Zone is a major NW-dipping normal fault comprising two fault strands, west and east (Figs. 2 and 3; Canora-Catalán et al., 2008). Paleo-seismic studies based on trench mapping of the two fault strands (Matthews Trench, Fig. 2; Fitzpatrick Trench, Fig. 3), regional fault mapping, and geomorphic analyses have revealed that the Whirinaki Fault Zone ruptured through to the surface at least eight times during the past 25 kyr, with single-event displacements ranging from decimeters to perhaps >2.5 m (Canora-Catalán et al., 2008, and references therein). Relevant here are the paleo-seismic results deduced from the Fitzpatrick Trench on

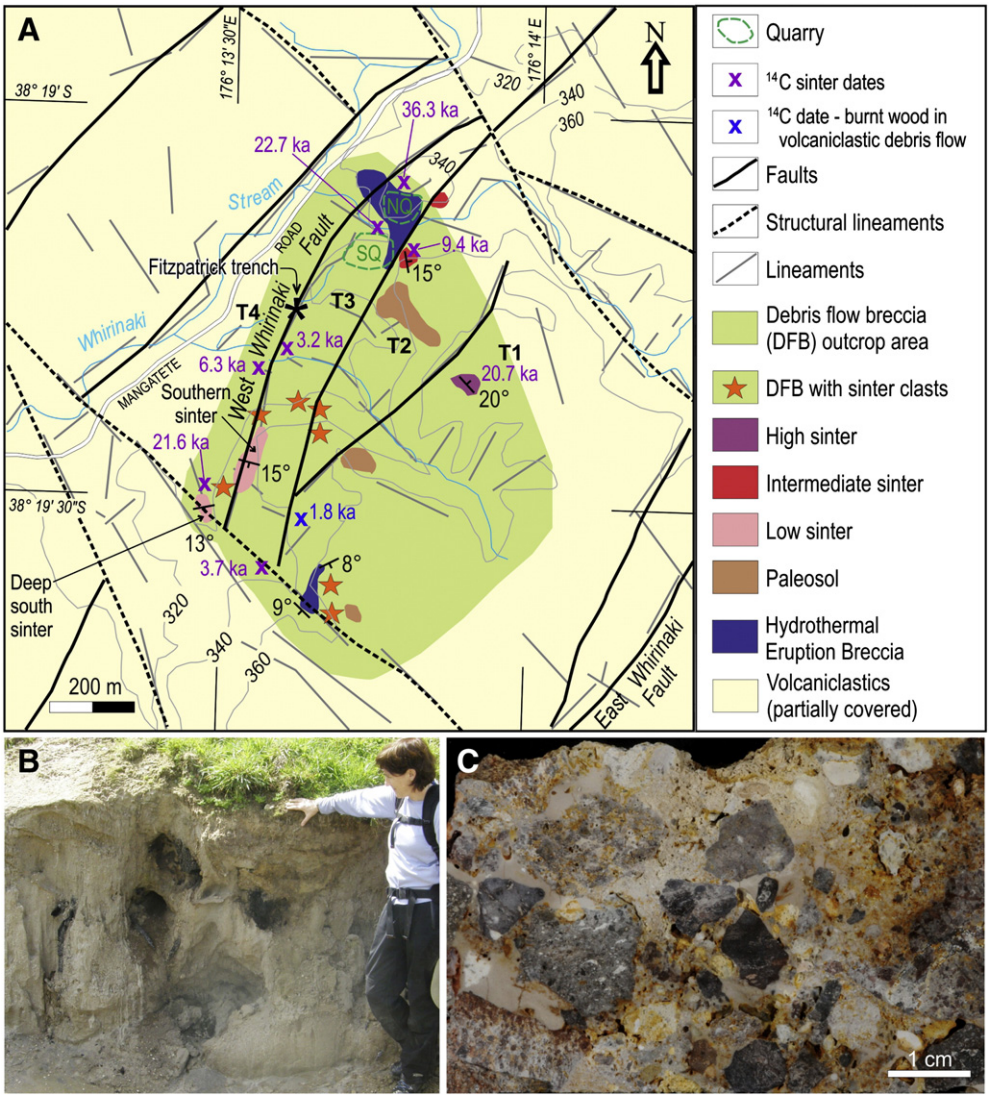

Fig. 3. Mangatete geological map and photographs of some local geological features in the study area. (A) The North and South Mangatete quarries (NQ and SQ, respectively; dashed dark green lines), and the West Whirinaki Fault, as well as its splays and parallel strands, together expose the local stratigraphy, including *in situ* siliceous sinter, paleosols, and breccias, the latter inferred herein to have been derived from hydrothermal eruptions. T1–T4 identify terraces in descending elevation to the west. *Ex situ* sinters (red stars) also occur along faults and within a locally extensive debris flow breccia (DFB, light green). (B) Volcanic ash (Taupo eruption) with charcoal dated by AMS ^{14}C analysis at one location at ~1.85 kyr old, is locally present at the base of the DFB. (C) Hand sample of silicified breccia from the southern exposure contains angular, subrounded and rounded volcanic and volcaniclastic granules, pebbles and cobbles.

the West Whirinaki Fault (Fig. 3) located within the study area; these are discussed further in Section 7.3.

At Mangatete, the West Whirinaki Fault displays three major branches, as well as several shorter, parallel and sub-parallel lineaments (Fig. 3A), presumably fault splays. Four major fault-bound terraces (T1–T4) are transected by NW–SE trending lineaments associated with minor breaks in the terraces, and which channel two streams across the fault block (Fig. 3A). These lineaments suggest subsurface faulting orthogonal to the trend of the Ngakuru Graben. Sinters exposed on the terraces are designated high, intermediate and low according to their elevation (Fig. 3A).

The North Quarry (Fig. 4A) provides conglomerate for local road fill. The site is also littered with cobbles and boulders of sinters and silicified tree fragments, many of which are hydrothermally altered (limonite-, hematite-stained). The South Quarry (Figs. 4A and 5A) lies ~10–15 m stratigraphically below the North Quarry, and ~100 m to the SSW, and is positioned upon a 25-m-high exposure of Late Quaternary lacustrine strata that has been thermally altered to zeolite (Brathwaite, 2003; discussed further in Section 7.2). Above the paraconformable top of the lacustrine deposits are outcrops of conglomerate, paleosols (Fig. 5B), and a sinter (Fig. 5C) comprising a distinctive packed fragmental texture (detailed in Section 5.2).

Approximately 450 m south of the South Quarry, the West Whirinaki Fault exposes a ~100-m-long sinter deposit (Fig. 3A, Southern sinter) consisting primarily of sinter blocks dislodged from the footwall of the fault. It also contains limited exposures of *in situ* sinter deposited unconformably upon a silicified paleosol. About 170 m S of the Southern sinter, the major splay of the Whirinaki Fault terminates at an orthogonal, NW–SE lineament (Fig. 3A), evident as a narrow valley with a normally dry watercourse at its base, discharging to the NW. Fifty meters NW of the junction of the lineament with the fault is the Deep South sinter (Fig. 3A), which comprises a 5-m-high vertical succession of interbedded clays, silicified paleosols and sinter. Surface exposures of sub-horizontal, laterally discontinuous deposits of silicified paleosols and sinters occur over an area some 80 m long × 60 m wide, with an extended distribution east beneath a debris flow deposit, toward the footwall. Specifically the siliceous deposits are partly overlain by a widespread, unconsolidated, matrix-supported, heterogeneous association of loose blocks, cobbles and small boulders of lacustrine, volcaniclastic and conglomeratic lithologies, forming a debris flow deposit (Fig. 3A),

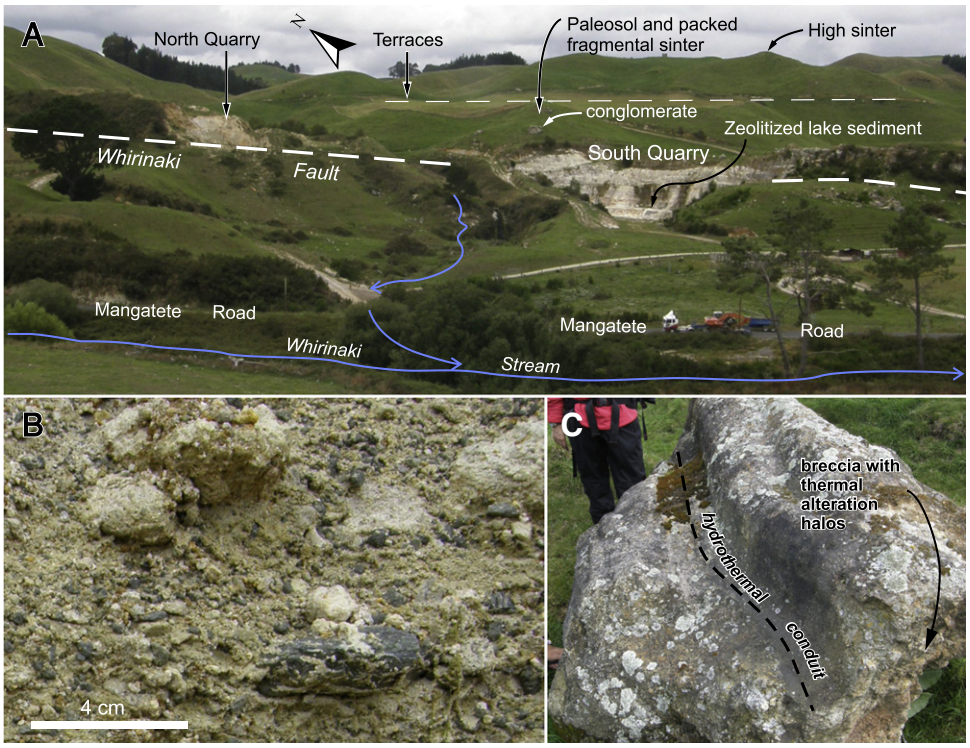

Fig. 4. Visual overview of the Mangatete field area and detail of the northern breccia. (A) View facing east showing the North and South quarries at Mangatete, which outcrop along the upthrown side of the West Whirinaki Fault, a prominent local structure (Villamor and Berryman, 2001) oriented parallel to the SW–NE tectonic grain of the TVZ rift axis. Fault terraces expose Mangatete sinters and paleosols at high, intermediate and low elevations (Fig. 3). These deposits overlie zeolitized lake sediments visible in the South Quarry. (B) Detail of unsilicified, poorly sorted breccia exposed in the North Quarry. (C) Indurated breccia block positioned near the South Quarry, displaying a sinuous, conduit-like, "negative" feature. A thin (few millimeters), mammelated, iron/silica cement lines the conduit.

the source of which is unknown. The debris deposit contains numerous sinter boulders and cobbles, and within its basal portion contains ash, charred tree branches, and charcoal (Fig. 3B).

3. Laboratory methods

Representative samples of Mangatete rock types, including sinters, were collected throughout the study area for further examination at the University of Auckland using optical microscopy, X-ray powder diffraction (XRD), and environmental scanning electron microscopy (ESEM). XRD analysis followed procedures outlined in Herdianita et al. (2000a). In brief, untreated samples were ground with a mortar and pestle, and the powder mounted in standard $20 \times 10 \times 1$ mm aluminum holders. A Phillips PW1130 X-ray diffractometer was operated at 40 kV and 20 mA, using CuKα radiation ($\lambda = 1.5405$), with a Phillips PW1050/25 goniometer fitted with a PW1752 curved graphite crystal monochromator and a PW1965 proportional detector. Samples were scanned at 0.6°2θ/min, with a step size of 0.01°, from 10–40°2θ. ESEM samples were examined using a FEI Quanta 200 F field emission gun with a SiLi (Lithium drifted) EDS detector and a Super Ultra Thin Window. Data acquisition was controlled by Sietronics (1993) VisXRD computer software.

Representative samples of sinters containing organic matter and a piece of charred wood were sent to the Rafter Radiocarbon Laboratory, National Isotope Centre, GNS Science, Lower Hutt, New Zealand, for accelerator mass spectrometry (AMS) ^{14}C dating. Possible organic contamination of sinter samples was minimized by soaking in hydrogen peroxide solution to remove exterior weathered surfaces. Subsequently the samples were cut, washed in dH_2O, dried, and crushed in a ring mill to ~5 mm size. Crushed sinter was treated with hot 10% HCl, and dH_2O washes. Samples were then digested in 50% HF, and allowed to sit for several days, adding fresh HF as required. The residue was washed with 3× hot 10% HCl, then 2× dH_2O. Floating plant fragments were collected, and the residue filtered at 150 μm. The >150 μm fraction was predominantly mineral or sinter fragments. The <150 μm fraction was sieved at 6 μm. Microscopic examination showed that the dark $6 < x < 150$ μm fraction had plant fragments and a few palynomorphs mixed into the mineral layer, and thus was chosen for dating. The sample fraction was transferred to a 6 mm combustion tube, converted to graphite by reduction with hydrogen over an iron catalyst, and the graphite was then measured on a tandem accelerator. The reported age is the conventional radiocarbon age before present (BP), calibrated on OxCal 4.2 (https://c14.arch.oc.ac.uk/oxcal/OxCal.html) using the SHCal13 dataset (Hogg et al., 2013). Calibrated ages are presented as mean ages with 2 sigma (95%) confidence limits (Table 1).

4. Mineralogy

Previous work has identified a consistent diagenetic progression of silica phase minerals within sinters, from noncrystalline opal-A to microcrystalline quartz (e.g., Herdianita et al., 2000a,b; Campbell et al., 2001; Lynne and Campbell, 2003, 2004; Jones and Renaut, 2007; Lynne et al., 2007). Herdianita et al. (2000b), their Fig. 8, p. 59) suggested that when the full width of the ~4 Å X-ray band at half maximum intensity (FWHM) is plotted against the age of a sample, two diagenetic pathways are apparent, with those sinters containing minerals other than silica or with high organic content converting more rapidly to quartz. Sinters at Otamakokore (also known as Whirinaki, Holland, 2000) and at Tahunaatara (Buddle, 2002; Campbell et al., 2004), both situated in the Ngakuru Graben (Fig. 2), follow the trend noted by Herdianita et al. (2000b) for a range of sinter ages from several locations. However, the Mangatete sinters plot outside this grouping (~18 ka to ~8 ka, and FWHM from 7.01 to 10.47; Fig. 6A), suggesting there is no consistent temporal trend in silica phase diagenesis in relation to the FWHM of the opal-A sinter trace.

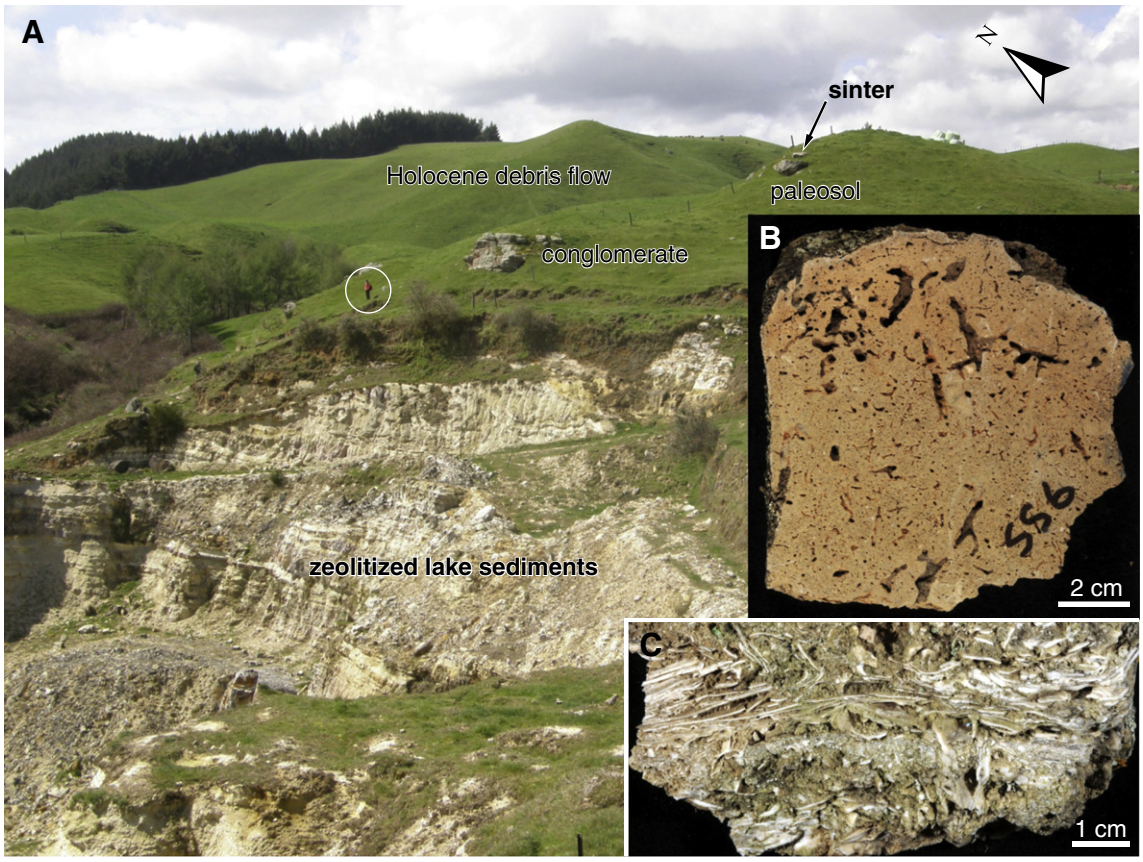

Fig. 5. Detail of the field stratigraphy of the South Quarry at Mangatete. (A) Zeolitized lake sediments disconformably overlain by a fluvial conglomerate, a silicified paleosol with root molds (B), and sinter near the top of the hill. Person circled to indicate scale. The *in situ* sinter above the South Quarry comprises a packed fragmental texture (C) described in Section 5.2, and its origin discussed in Section 7.1.

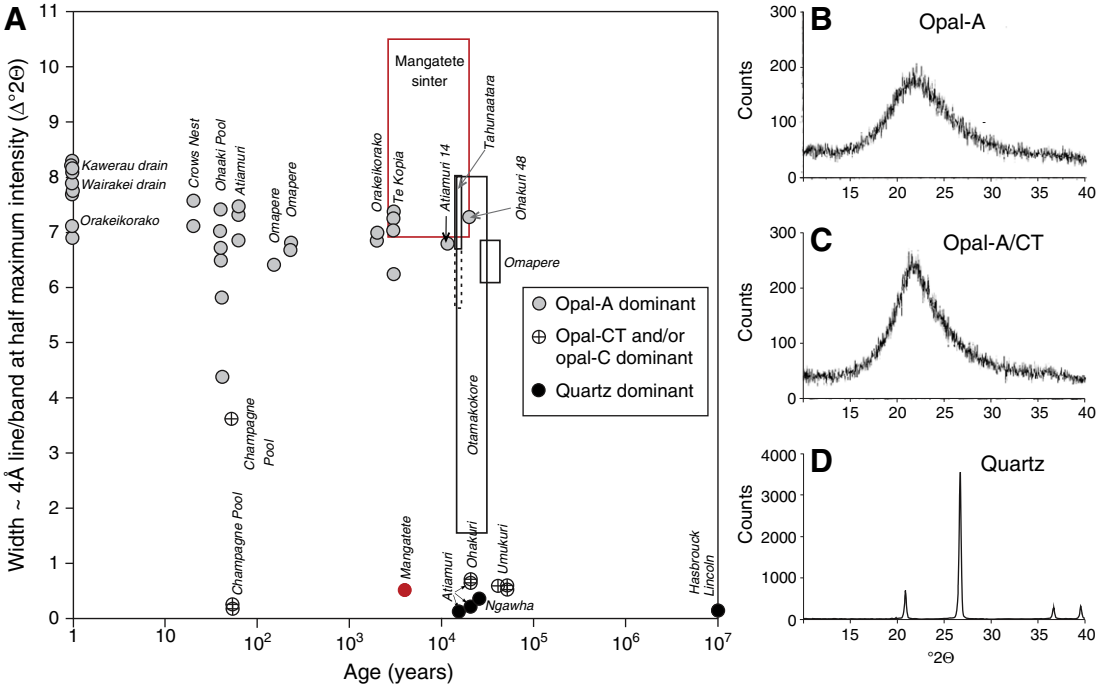

Fig. 6. X-ray powder diffraction data for selected Mangatete sinter samples. (A) Full width at half maximum intensity of the ~4 Å line as a proxy for crystallinity *versus* estimated ages of sinters from the TVZ and elsewhere (modified from Herdianita et al., 2000b). Mangatete sinter ranges outlined by red box and quartzose sample indicated by red circle. Discussed further in text. (B) Typical opal-A trace. (C) Typical opal-A/CT trace. (D) Typical quartz trace.

Most of the 29 sinter samples collected from Mangatete for this study constituted noncrystalline opal-A (Fig. 6B). Exceptions include three samples exhibiting incipient transformation to opal CT (Fig. 6C), and two sinter blocks — a stromatolite (Fig. 7A) and a conical tufted sinter — composed of microcrystalline quartz (e.g., Fig. 6D). Therefore, silica phase maturation at Mangatete is largely nascent, in strong contrast, for example, to Sinter Island in Lake Ohakuri (Fig. 2; Campbell and Lynne, 2006) situated approximately 18 km SW of Mangatete, where maturation to microcrystalline quartz took place in less than 500 years. Hence, we are reminded that the factors influencing the rate of silica diagenesis in sinters remain unclear.

Mineral products of hydrothermal alteration (hematite, wairakite, wüstite and kaolin) were present in the XRD traces in only minor amounts. Wairakite may derive from lithologies that were originally more deeply buried and then ejected in a hydrothermal eruption, as this mineral is not known to form below a temperature of 210 °C (e.g., Giggenbach, 1984). Kaolinite and wüstite most likely formed as alteration products of near-surface acid steam condensate (e.g., Browne, 1978).

5. Lithofacies of hydrothermally related deposits at Mangatete

Two types of hydrothermal eruption breccias—unconsolidated and silicified—are inferred from localized, coarse volcaniclastic deposits that occur within the study area (Section 5.1). In addition, nine sedimentary facies were identified in Mangatete sinters (Sections 5.2–5.4; Figs. 7 and 8). Five imply typical mid- to low-temperature (~55–30 °C), near-neutral pH, alkali chloride discharge apron, terrace pool, or thermal stream conditions (Fig. 7), as described in Section 5.2 and discussed further in Section 7. Some interpreted alkali chloride sinters, in particular highly porous, wavy tufted, network and bubble mat textures, show signs of post-depositional acid steam condensate overprinting (Fig. 8A–C) in the North Quarry area, as described in Section 5.3 and discussed in Section 7. Moreover, four unusual siliceous fabrics (globular, vuggy, scalloped and arcuate layered; Fig. 8D–G) are texturally unlike sinters deposited under alkali chloride conditions. They instead appear to be related to mixed acid-sulfate-chloride thermal fluids, possibly associated with fossil fumaroles also situated in the North Quarry area, as described in Section 5.4 and discussed further in Section 7.

5.1. Hydrothermal eruption breccias

Coarse volcaniclastic deposits, both unconsolidated and silicified, occur in the northern and southern parts of the Mangatete study area. No vents have been identified in the field area, and the extent of these breccias cannot be determined because of widespread cover by overlying deposits and pastureland. However, the breccias that are exposed possess textural and compositional characteristics akin to the products of hydrothermal eruptions. The North Quarry breccia (Fig. 4B) is a matrix-supported mixture of unsilicified, poorly sorted, mainly subrounded to sub-angular cobbles and pebbles of mixed compositions (clays, various volcanics, volcaniclastics and reworked conglomerates), in an unconsolidated matrix of clay and sand. Poorly defined, horizontal to sub-horizontal bedding planes separate vague layers of alternating coarse cobbles and pebbly sands, some of which pinch out laterally. The beds are not graded, and there is no overall nor repeated stratigraphic pattern evident in the quarry face.

The rounding of pebbles could indicate abrasion due to fluvial transport, but the degree of rounding is also consistent with milling in the funnel of a hydrothermal eruption vent (Browne and Lawless, 2001). We identify this deposit as a hydrothermal eruption breccia (HEB) because of its very poor sorting, the presence of matrix-supported clasts of heterogeneous lithology, and its position in an active geothermal zone. The breccia also lacks typical fluvial features such as cross-bedding/lamination, foresets, strong sorting or graded bedding, as occur associated with the nearby Tahunaatara and Otamakokore sinters (Holland, 2000; Buddle, 2002; Campbell et al., 2004). Moreover, the Mangatete paleo-hydrothermal system is situated in a region typified by extensive hydrothermal eruption deposits (Fig. 2). However, it differs from known HEBs in the Ngakuru Graben area (e.g., Parsons Road HEB, Frying Pan Lake HEB at Waimungu; Fig. 2), which contain much larger clasts (up to boulder size, and thus indicate vent proximity) and matrix sediments that are up to ~80% clay in composition. The lack of cementation of the clasts in the North Quarry deposit indicates that silica-saturated thermal fluids did not later infiltrate the breccia. The indistinct bedding implies a succession of surges or eruptions (cf. Waimungu hydrothermal eruption of 1917, as described in Simmons, 1995). At Mangatete, an out-of-place, 1.8-m-long boulder near the South Quarry preserves a probable HEB conduit structure (Fig. 4C).

The Southern HEB (Fig. 3C) constitutes a partly clast-supported, poorly sorted, silicified breccia of sub-angular pebbles (5–40 mm), with the cement showing swirly, irregular patches of red and yellow alteration, indicative of post-depositional alteration by acidic fluids depositing hematite and jarosite, respectively. The larger clasts themselves contain some matrix-supported conglomerates with mm-sized, angular to sub-rounded grains of mixed lithology (e.g., volcanics, volcaniclastics). Strong cementation implies the eruption was accompanied or succeeded by infiltration of silica-saturated thermal fluids.

5.2. Siliceous sinter facies formed in alkali chloride springs

The five inferred alkali chloride sinter facies at Mangatete are described briefly below.

(1) *Domal stromatolitic*. A wavy laminated to domal stromatolitic texture (Fig. 7A, B) occurs in scattered, *ex situ* sinter clasts in the southern portion of the study area. It likely formed in relatively deep (>1 m), quiescent, mid-temperature (~45–55 °C), mid-apron pools (compare to Fig. 9A). One sample (Fig. 7A) yielded an AMS ^{14}C date of 3730 ± 50 cal yr BP. It is one of the youngest sinters dated at Mangatete, and yet is one of only two samples analyzed where diagenesis has progressed to microcrystalline quartz (Fig. 6D; Section 4). Some cobbles of wavy laminated to domal stromatolites contain numerous small fenestrae (Fig. 7B), inferred to represent photosynthetic degassing of subaqueous microbial mats (cf. Hinman and Lindstrom, 1996). Conical tufts and fine wavy laminae (Fig. 7C) are evident at the microscale.

(2) *Tufted sinter with lenticular voids*. Strongly wave-form, large (up to 20 cm vertical relief) conical tufts with lenticular voids ("bubble mats") and network fabrics occur in the North Quarry area (Fig. 7D). Such features are common in mid-temperature (~45–55 °C), mid-apron pools in modern hot springs, reflecting cyanobacterial (e.g. *Leptolyngbya*) phototaxis and trapped oxygen bubbles derived from photosynthetic mat exudates (cf. Lynne, 2012; her Fig. 6A, p. 11).

(3) *Packed fragmental sinter* was sampled from the top of the South Quarry (Figs. 5C and 7E), and also was found in several locations in the Deep South sinter. Initially observed in Jurassic sinters in Patagonia (Guido and Campbell, 2011, their Fig. 5D, p. 43), at Mangatete the facies comprises a pale brown, porous siliceous matrix bristling with prominent white sinter flakes up to 12 × 6 mm in diameter. The flakes are angular, irregular in outline, but approximately rectangular to polygonal in shape, and stacked in moderately abundant to dense arrays. They are paper thin but moderately strong. The matrix consists of small pale brown sinter flakes decreasing in size, set in a groundmass of sub-millimeter silica spheres. During the course of this study, a modern analog was identified in the point bars of Hot Water Creek, Waimangu Volcanic Valley (Figs. 2 and 9B–G), as discussed in detail in Section 7.1.

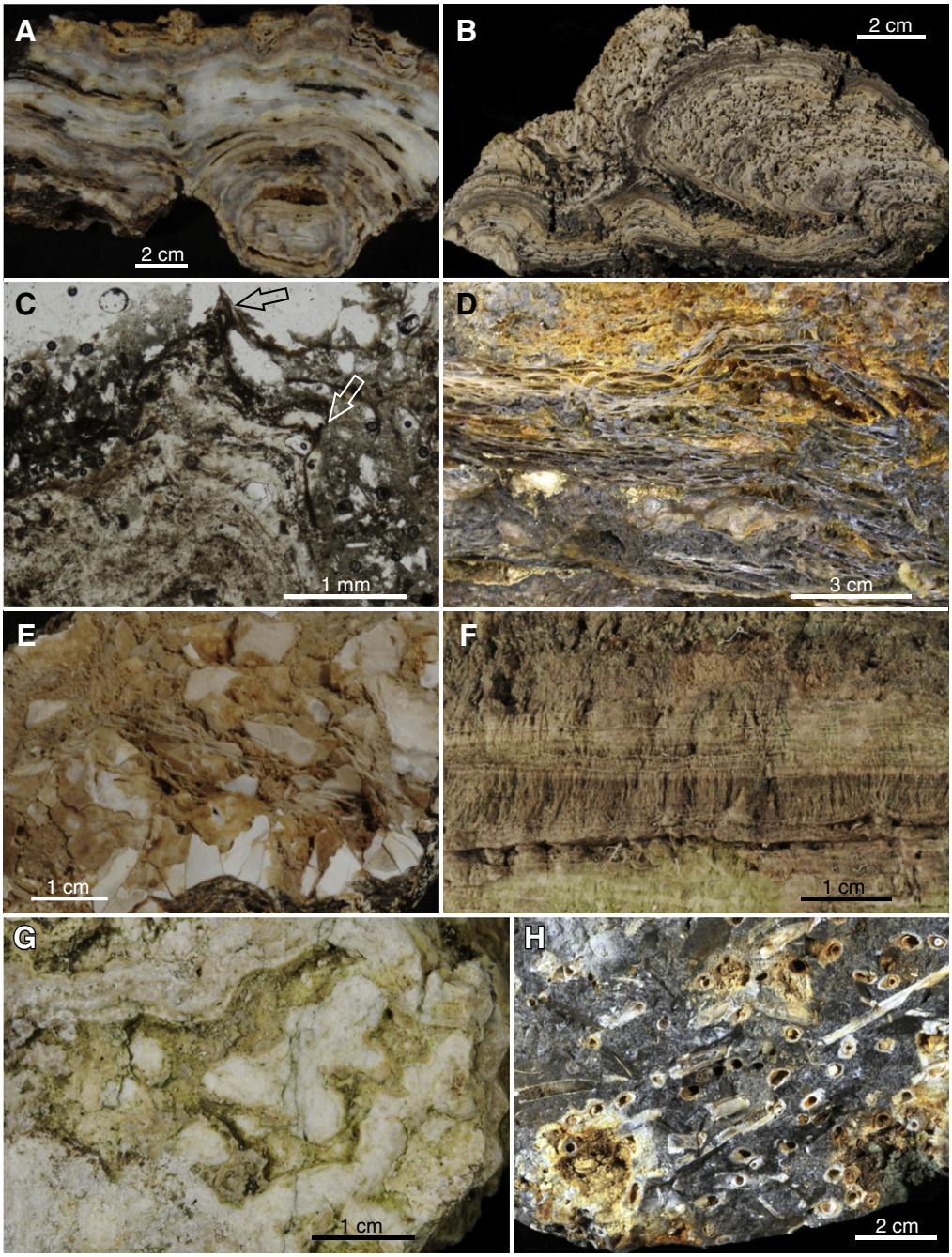

Fig. 7. Siliceous sinter fabrics at Mangatete characteristic of near-neutral pH, alkali chloride thermal discharge. All rock slabs were photographed in vertical orientation unless otherwise noted. (A) Wavy to broadly domal stromatolitic; *ex situ* block collected adjacent to southern silicified hydrothermal eruption breccia (Fig. 3), and ^{14}C dated at 3.7 ka. (B) Curved domal stromatolite with numerous small fenestrae; *ex situ* cobble collected on eastern parallel splay of Whirinaki Fault (Fig. 3A). (C) Detail of (B) showing both clotted (dark) and wavy laminated, conical tufted fabric (arrows indicate tuft tips). (D) Large amplitude wavy tufts, network fabric and lenticular voids (i.e. flattened bubbles trapping photosynthetically produced gas), typical of mid-temperature (~55–45 °C) apron discharge channels. (E) Oblique plan view detail of packed fragmental sinter texture collected from the top of the South Quarry (Fig. 5A, C) illustrating stacked nature of the white, thin, indurated sinter flakes and their angular shapes. (F) Coarsely filamentous palisade fabric comprising layers (~1 cm thick) of silicified, shrubby, vertical micro-pillar structures, shown in modern hot springs to represent cyanobacterial (*Calothrix*) mats growing in warm (~40–30 °C), shallow terracette pools (e.g. Walter, 1976; Cady and Farmer, 1996; Guido and Campbell, 2011; Lynne, 2012). (G) Plan view of palisade terracette exhibiting a pustular, vaguely mammelated relief on its top surface, surrounded by a terracette rim. Sample collected as *ex situ* clast on West Whirinaki Fault adjacent to the Southern sinter (Fig. 3A). (H) Silicified reeds and reed molds, broadly aligned, showing primary porosity in some stems; preserved in a dark gray, porous, siliceous matrix. This is a common fabric in thermally influenced wetlands (Guido and Campbell, 2011, and references therein).

(4) Coarsely filamentous *palisade sinter* (Fig. 7F), with individual stacked horizons of vertical pillars on the order of ~1 cm thickness, is common along the trace of the West Whirinaki Fault in southern Mangatete, with one *ex situ* clast dated by AMS ^{14}C methods at ~3 ka. Some bedding plane-oriented samples display pustular fabric in arcuate terracettes (Fig. 7G), typical features formed by modern cyanobacterial mats of *Calothrix* at low temperatures (<45 °C) on distal sinter apron terraces (Cady and Farmer, 1996; Guido and Campbell, 2011).

(5) *Plant-rich sinters* (Fig. 7H) are very common at Mangatete; AMS ^{14}C dating yielded a range in sample ages from 36.3 ka to 20.7 ka. They are packed with randomly to parallel-oriented, silicified reeds (to 4-cm-long) set in a fine-grained, porous, siliceous matrix, and they commonly overlie or are otherwise associated

with silicified paleosols (Fig. 5A, B). Plant-rich sinters form today at the limit of influence of thermal fluids, in close spatial association with thermal marsh or fen habitats (Channing et al., 2004; Channing and Edwards, 2009).

5.3. Acid thermal fluid overprinting of pre-existing alkali chloride siliceous sinter

Evidence for acid overprinting of sinter at Mangatete is found in *ex situ* blocks of the North Quarry (Fig. 7D), where extensive red- and yellow-staining (hematite and jarosite, respectively) permeates the previously formed sinter textures that are indicative of near-neutral pH, alkali chloride, mid-temperature, apron terrace conditions, namely wavy conical tufts with bubble mats and network fabrics (Fig. 8A). Presumably the originally high porosity of the primary sinter fabric made it especially susceptible to alteration by acid steam condensate filtering through the local strata. Cavernous secondary porosity developed in the tufted/network fabrics (Fig. 8B), and acid-etching formed innumerable dissolution pits at the micron scale (Fig. 8C). Similar dissolution of primary sinter fabrics is evident in Subrecent geyserites exposed around inactive geyser vents at the Whakarewarewa (now Te Puia) thermal area, Rotorua, which are being subjected to fumarolic overprinting today (Jones and Renaut, 2003, their Figs. 11 and 12, pp. 1599–1601). While rapid conversion of noncrystalline opal to microcrystalline quartz has been reported in sinters from some areas undergoing acidic steam overprinting (e.g., Campbell and Lynne, 2006; Lynne et al., 2006), all analyzed North Quarry sinters showed only opal-A or opal-A/CT silica mineral phase signatures (Section 4).

5.4. Siliceous sinters formed in association with acidic springs

Locally restricted (meters to up to a few tens of meters in extent) and thin (a few centimeters to decimeters thick), acid sinter deposits have been described from a few modern acid-sulfate-chloride hot springs in the TVZ (Jones et al., 1999a,b, 2000; Mountain et al., 2003; Letelier, 2004; Schinteie et al., 2007; Jones and Renaut, 2012). They are characterized by markedly lower silica precipitation rates (Mountain et al., 2003) than the better known alkali chloride sinters of generally greater areal extent and thickness (up to several square kilometers in area and up to tens of meters thick). Texturally in outcrop and hand samples, modern acid sinters are characterized by broadly wavy and layered silicified pavements, ledges and ramparts, as well as by spicular textures within siliceous rims around hot pools or atop pumice clasts (e.g., Letelier, 2004; Schinteie et al., 2007; Jones and Renaut, 2012). Oncoids also develop in very shallow (few centimeters depth), acid-sulfate-chloride spring discharges, and may be distinguished from alkali chloride spring-derived oncoids by their biotic content (Jones et al., 1999a,b). At the microscale, acid sinters precipitate smaller and more irregular opaline silica spheres, with primary and secondary corrosion and pitting common at all scales (Rodgers et al., 2004; Schinteie et al., 2007). Similar dissolution features to these modern TVZ examples also were observed at Mangatete. Although modern acid sinters could potentially be confused with silica residue, the latter are very thin (millimeters to few centimeters thick), and constitute spatially very patchy, irregular deposits that originate from largely destructional processes, specifically remobilization and reprecipitation of silica derived from the dissolution of country rock in areas of steaming ground and fumaroles (Rodgers et al., 2002, 2004). Acid sinters have gone virtually unrecognized in the geological record (White et al., 1964; Murphy, 2013), but are likely to be far more common than is currently known. To date, their obscurity may be attributed to a paucity of clear criteria for their recognition. Moreover, the overall acidic environmental conditions under which they form may create an inherent taphonomic bias hindering the long-term preservation potential of acid sinters. At Tikitere (Hell's Gate) geothermal field, NE of Rotorua, TVZ, we have observed dried (inactive/Subrecent), relatively thin deposits of acid sinters breaking up and eroding on exposed surfaces, or "rotting" near active fumaroles.

In boulders and clasts of the North Quarry at Mangatete, four unusual primary sinter fabrics (Fig. 8D–G) are attributed herein to parent paleothermal fluids of mixed acid-sulfate-chloride composition. These acid sinter textures are described below, and their paleoenvironmental significance discussed further in Section 7.1.

(1) *Vuggy fabric*. Sinuous channels (centimeters wide × tens of centimeters long) and large vugs (Fig. 8D) meander through a heterolithic, pebble-sized breccia cemented by silica and, in places, stained black in thin linings around vug interiors, inferred to have been formed from escaping sulfur-laden gases in fossil fumaroles. Tikitere hosts numerous fumaroles and black sulfur mound deposits (Letelier, 2004; personal observations) that may serve as modern analog settings for the formation of similar fossil features at Mangatete.

(2) *Globular sponge fabric*. A globular, spongy, dark gray, siliceous sinter fabric with subrounded vugs is lined with yellowish to orange iron-stained silica, or partly filled with fine-grained, light gray siliceous geopetals (Fig. 8E). There are more solid silica areas than pores in this fabric type. The vugs are irregular in size and orientation; the walls (~3 mm thick) are bulbous, giving an overall globular appearance. The bluish gray matrix consists of non-crystalline opal-A. While we know of no modern analog for this fabric, we suggest it may be the result of alternating emanations of vapor and silica-charged liquid immersion, with the overall vuggy and dissolved appearance (cf. Schinteie et al., 2007) suggestive of formation in an acidic setting.

(3) *Scalloped fabric*. This fabric (Fig. 8F) constitutes an overall irregularly scalloped texture in plan view (~4 cm diameter) comprising wavy, stacked siliceous laminae in cross-sectional view (up to 15 cm thick).

(4) *Arcuate, wavy layered fabric*. Arcuate, wavy, thinly layered, dark gray to reddish stained, fine-grained siliceous deposits (Fig. 8G) traverse volcaniclastic sands in sinuous bands throughout North Quarry *ex situ* boulders.

6. Dated sinter sample characteristics, locations and ages

One piece of charred wood and seven sinter samples were chosen for AMS ^{14}C dating to represent typical deposits from the four terraces (T1–T4) in the Mangatete study area (Fig. 3A, Table 1). In addition, Brathwaite (2003) reported a radiocarbon date (recalibrated to 9.4 kyr BP; see Section 3) for a packed fragmental sinter (PFS) sample (S4, Table 1), termed the Intermediate sinter herein, which is located above the South Quarry on T2 (Figs. 3A and 5A). The dated charcoal sample (1.8 ka) was entombed in ash at the base of the Holocene debris flow deposit on T1 (Fig. 3B). The age determinations, terrace position, lithofacies, mineralogy and inferred setting of the analyzed samples are summarized in Table 1. Sample locations and ages also are marked on the geological map of the study site (Fig. 3A). A brief descriptive summary of relevant aspects of the dated sinter samples follows here.

The oldest sinter date was obtained from a float block of dark, plant-rich sinter collected on T3, from the summit above the North Quarry (S8, 36.3 ka). All North Quarry sinter samples occur as float blocks and most have undergone post-depositional hydrothermal alteration, but their original paleoenvironmentally significant textures remain intact (Section 5). In addition, one *ex situ* and two *in situ* sinter samples were collected from widely scattered locations in the study area (S5–S7; Fig. 3A, Table 1), but are of similar age (22.7–20.7 ka) and facies type. They are characterized by layered, fine-grained, dark gray sinter with plant reeds and molds and occasional thin (~1 cm thick), white silicified ash horizons. At Mangatete, plant-rich sinters typically are associated with sub-horizontal, laterally discontinuous exposures of silicified paleosols. Packed fragmental sinter was sampled

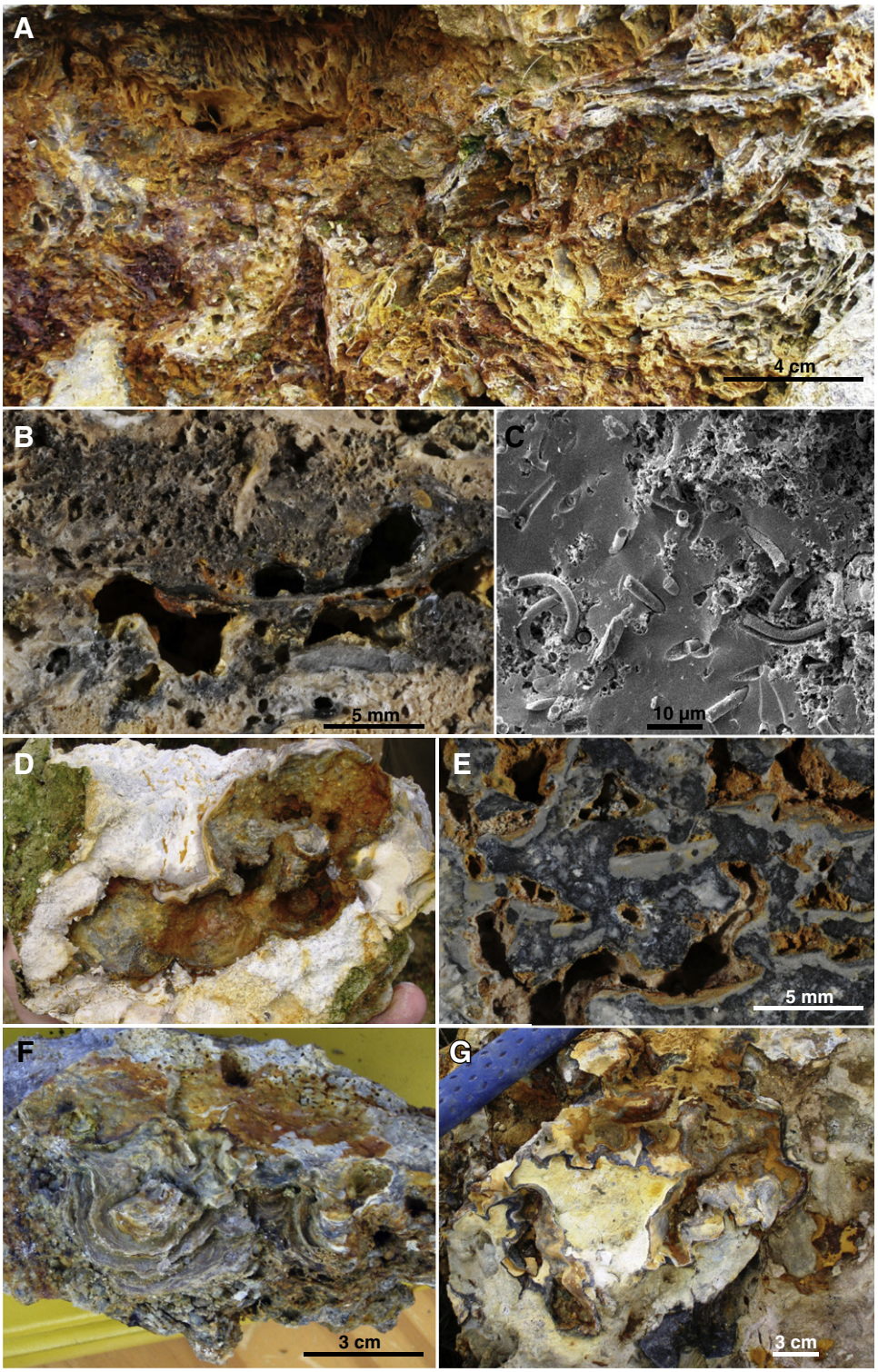

Fig. 8. Siliceous fabrics preserved in *ex situ* blocks in the North Quarry at Mangatete, suggestive of acid-overprinting of originally alkali chloride spring-deposited sinters (A–C), or interpreted to have formed as primary deposits in acid-sulfate-chloride thermal springs (D–G). (A) Vertical section of wavy, tufted, siliceous sinter, with lenticular voids somewhat enlarged by dissolution and stained by hematite (red) and jarosite (yellow). (B) Detail of (A) in a cut slab showing wavy network fabric with etched voids. Vertical section view. (C) Scanning electron micrograph of (B) revealing silicified filaments (~2 µm diameter) in vitreous siliceous matrix containing rough, corroded, naturally acid-etched patches. (D) Plan view of hand sample preserving an inferred, small fumarole (i.e. the central, sinuous, reddish gray vug), surrounded by white, botryoidal, massive silica. (E) Globular sponge fabric in vertical section view, comprising a dark gray siliceous matrix with numerous small, irregular vugs partially filled, in places, by light gray siliceous geopetal sediments. Fabric implies both dissolution and precipitation, possibly in a setting where acidic vapor phases alternated with hot silica-charged liquids passing through the porous deposit. (F) Plan view of distinctly but irregularly scalloped siliceous fabric, aggraded in mm-thick layers, suggesting a pool margin setting (compare to Fig. 9H). (G) Oblique plan view of broadly and irregularly arcuate, layered silica (gray), meandering through massive, white to orange, iron-stained silica (compare to Fig. 9I).

atop a paleosol above the South Quarry (Fig. 5) and dated at 9.4 ka; the same texture also was found in the Deep South sinter deposit. Moreover, the Southern HEB (Section 5.1) is positioned on T1 and is strongly silicified (Fig. 3C), indicating infusion with silica-saturated fluids concomitant with or subsequent to the hydrothermal eruption, the timing of which is unknown. An ~11 kyr duration break in sinter ages (Table 1) may be the product of incomplete sampling, signify erosion of the sinter record from this time interval, or demarcate temporary cessation of hydrothermal activity in the Mangatete area. Subsequently the youngest, unaltered sinter record from T2 to T4 (6.3–3.1 ka, Table 1) constitutes a variety of *in situ* and *ex situ* sinter textural types representing mid- to low-temperature hot spring pools, hot-water streams or discharge aprons (Sections 5.2, 7.1).

7. Discussion

7.1. Paleoenvironmental significance of Mangatete sinter fabrics

Very high temperature geothermal facies—geyser vent, proximal slope and upper channel (Cady and Farmer, 1996; Lowe et al., 2001; Lynne, 2012)—are not exposed in the Mangatete paleo-geothermal system, and may have eroded after faulting occurred. The preserved alkali chloride sinters contain fossil microbial fabrics and plants (Fig. 7), similar to those reported from Jurassic sinters in Patagonia (Guido et al., 2010; Guido and Campbell, 2011), Quaternary Yellowstone hot-spring systems (Hinman and Lindstrom, 1996; Guidry and Chafetz, 2003b), and of Quaternary sinters elsewhere in the TVZ (Campbell et al., 2001, 2004). Fossil plants and microbial fabrics also are well represented in Devonian sinters of Australia and Scotland (Walter et al., 1996; Trewin et al., 2003). These sinter fabrics—domal stromatolitic (e.g. cf. Figs. 7A, B and 9A), conical tufted/network, palisade, and silicified reeds—are typical of mid- to low-temperature pools of near-neutral pH, alkali chloride spring discharge aprons and terraces, as well as of surrounding thermally influenced wetlands (Section 5.2). One sinter facies type from Mangatete—packed fragmental—is new and warrants further analysis.

Packed fragmental sinter (PFS) was recognized recently in Jurassic sinters of Argentinean Patagonia and there inferred as broken, silicified microbial mats, transported in thermal spring-fed streams, and ultimately deposited in point bars (Guido and Campbell, 2011). In a search

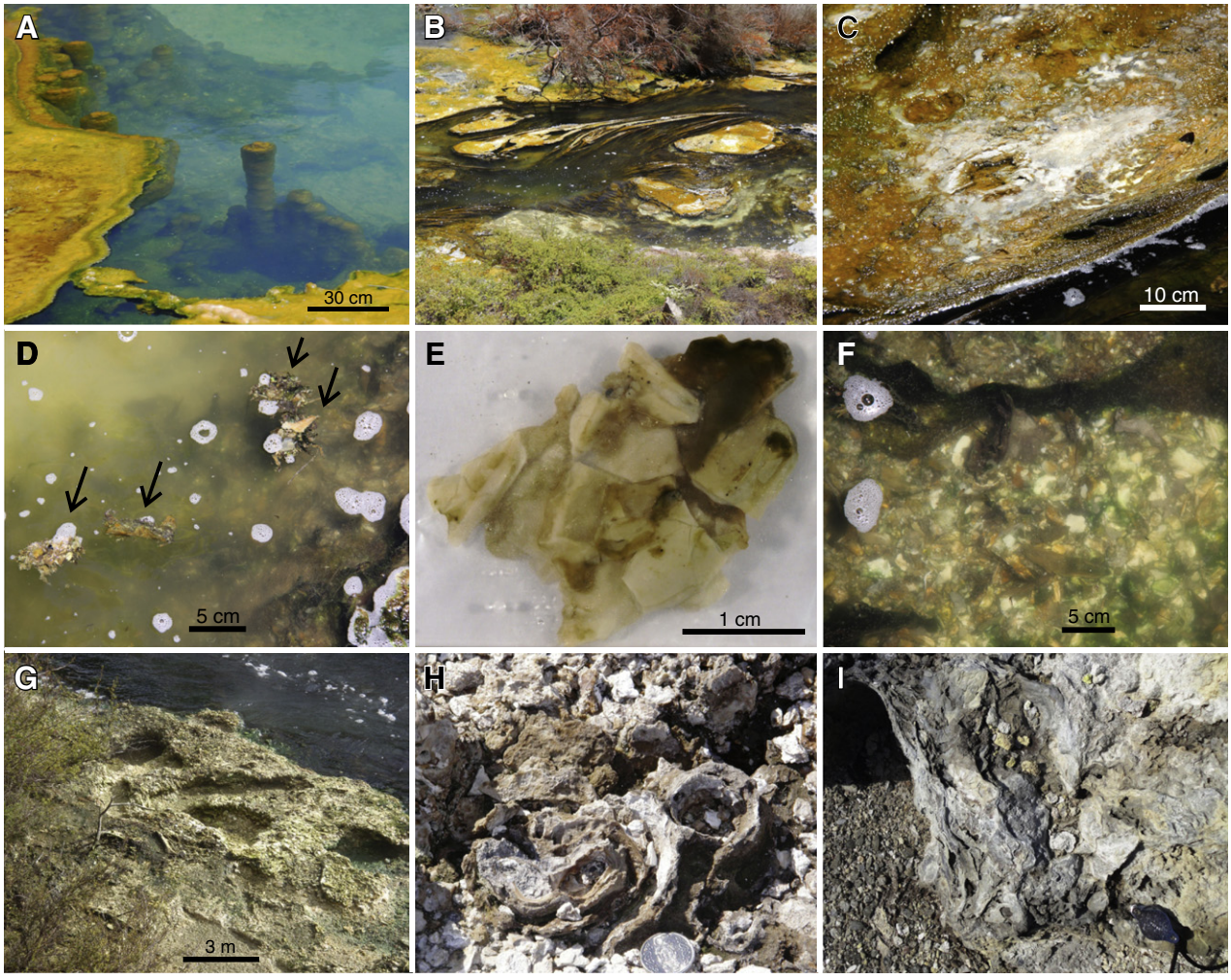

Fig. 9. Modern analog textures and geothermal settings for selected Mangatete sinter facies: (A–G) alkali chloride sinter fabrics; (H-I) sinter fabrics from acid geothermal areas. (A) Domal to columnar, subaqueous stromatolites comprising green and orange cyanobacterial mats; from Map of Africa hot pool, Orakei Korako, TVZ, in moderately warm alkali chloride spring-fed pool (cf. Fig. 7B). (B) Hot Water Creek, Waimangu, flowing downstream to the right, showing thick mats of green (subaqueous) and orange (wet subaerial) cyanobacteria, fed by moderate temperature, alkali chloride springs discharging within and along the stream. Field of view 10 m. (C) Silicifying, drying orange cyanobacterial mat growing from the streambank as a sheet over the top of Hot Water Creek. (D) Torn green and orange bacterial mats clinging to ripped up, indurated sinter clasts floating downstream in Hot Water Creek after a storm. (E) Detail of flaky, white sinter "floater" (cf. Fig. 7E). (F) Close-up of Hot Water Creek floor in a still area, where the green subaqueous microbial mat has been eroded, and white sinter flakes subsequently have settled onto the bottom. (G) Light colored point bar along Hot Water Creek, one of many situated within 200 m of its outflow from Frying Pan Lake, constituting uncemented, densely packed, dried, white siliceous sinter flakes. (H) Circular and scalloped siliceous sinter layers along the margin of an inactive acid spring, Tikitere, TVZ (cf. Fig. 8F). Coin, 2 cm diameter. (I) Arcuate, wavy, siliceous sinter layers at the margin of an inactive fumarole, Rotokawa geothermal area (cf. Fig. 8G). Hand lens 3 cm wide.

Table 1
Dates and locations of sinter samples. Sample S4 was dated by Brathwaite (2003); others from this study are as described in Section 6. Conventional radiocarbon dates have been calibrated as described in Section 3, and are presented here as mean ages with 2 sigma (95%) confidence limits. Terrace numbers (tied to the geological and geographic map of Fig. 3A), and sample collection locations and ages also are shown in this table. "Figure" refers to representative sinter texture photographs presented in this paper. Minimal diagenesis has occurred in the oldest sinters (which also appear visually to be the most hydrothermally altered), and maximum diagenesis in the youngest. Hence, there is no consistent rate of silica maturation in Mangatete sinters with age. Sinter lithofacies indicate paleo-environmental settings from mid-apron slopes to distal terraces in relation to hot spring vents, with likely post-depositional erosion of proximal (vent) facies.

Field	Cal yr BP	Error ± cal yr BP	*in situ*	Terrace	Lithofacies	Figure	Silica phase mineral	Inferred setting
W	1845	30	Y	T1	Charred wood in volcanic ash	3B	_	burnt forest
S1	3150	55	Y	T3	Curved domal stromatolite with numerous fenestrae	6B	opal-A monocrystaline	deep mid-apron pool
S2	3730	50	N	T3	Wavy to broadly domal stromatolite	6A	quartz	deep mid-apron pool
S3	6345	45	N	T4	Palisade sinter	6 F	opal-A	distal terracette pool
S4	9420	60	Y	T2	Packed fragmental sinter	6E	opal-A	point bar on turbulent hot-water stream
S5	20,680	110	N	T1	Plant-rich sinter	cf. 6H	opal-A	distal apron
S6	21,625	125	Y	T4(T1*)	Plant-rich sinter	cf. 6H	opal-A	distal apron
S7	22,665	120	N	T3	Plant-rich sinter	cf. 6H	opal-A	distal apron
S8	36,320	490	N	T3	Plant-rich sinter	cf. 6H	opal-A	distal apron

for a modern analog throughout the TVZ, we located the formation process (Fig. 9B–G) of this distinctive texture at present day Hot Water Creek, Waimangu Volcanic Valley, ~18 km NE of Mangatete (Fig. 2). Frying Pan Lake (300 m × 200 m, 48–52 °C, pH 5.6–5.8; Jones et al., 2005) contains sublacustrine springs, bankside subaerial alkali chloride hot springs, and hosts cyanobacterial stromatolites growing upward from the shallow lake bottom to form living microbial "lilypads" at the surface (Jones et al., 2005). The 1.8-km-long outflow from Frying Pan Lake to Lake Rotomahana is *via* Hot Water Creek (Fig. 9B, ~2.4 m wide 200 m downstream from the lake outlet). Hot Water Creek is a fast flowing (average 110 l/s; Jones et al., 2005), warm stream fed by numerous hot springs mainly distributed along its northern banks. These thermal inputs ensure that the creek maintains temperatures of 51–67 °C and a pH of 3–8 (Jones et al., 2005). Thus, Hot Water Creek provides suitable conditions, especially in summer months, for luxuriant green and orange cyanobacterial mats to encrust its margins, to extend into the channel flow in long (up to 1 m) microbial streamers (Fig. 9B), and to grow outward over the creek surface in thin microbial sheets (Fig. 9C). Under relatively calm and dry conditions, white siliceous sinter forms at the basal portions of the streamers and within the floating sheets (Fig. 9C). Thick green and orange microbial mats, with pustules and trapped bubbles, line the channel sides and bottom. A white sinter armor of unknown thickness coats the subaqueous channel floor and bank margin areas beneath the mats, and is exposed in places where rapid turbulent flow has scoured out the mat-lined stream bed. Following heavy rainfall with increased flow in the channel, rip-up clasts of white silica flakes covered with dark microbial mats float down the creek (Fig. 9D). Silica flakes collected from these creek "floaters" (Fig. 9E) are identical in size and shape to the flakes in the fossil packed fragmental sinter facies of Patagonia and Mangatete. At Waimangu, we observed sinter flakes that had settled onto the creek bottom during quiet intervals, where it had been scoured and the mats removed (Fig. 9F). For several hundred meters along the channel from the lake outlet, the white flakes are densely packed vertically and horizontally to build up streamside point bar deposits (Fig. 9H). Thus, we verify that PFS signifies a narrow facies range—fast flowing, moderately hot (~50 °C), alkali chloride spring-fed streams sustaining cyanobacterial communities—and therefore this texture is useful in interpreting the paleo-hydrology of fossil geothermal systems.

The four other previously undescribed sinter fabrics reported herein from Mangatete—vuggy, globular spongy, scalloped and arcuate layered (Fig. 8D–G)—were found only in *ex situ* siliceous blocks of the North Quarry. They are similar to silica residue (Rodgers et al., 2002, 2004) in that they show dissolution features; however, unlike silica residue the texturally unusual Mangatete siliceous deposits are volumetrically significant, occurring as boulders and cobbles, and display distinctive physical sedimentary structures. Modern siliceous and sulfur/silica mounds of low relief (<0.5 m high) are common in parts of the Tikitere Thermal Area, TVZ, which is dominated by acid thermal manifestations. Similar, recently inactive, black S/Si features at Ngapouri (Fig. 2) display internal tortuous conduit channels of the same size and shape as the preserved Mangatete fabrics (personal observations). While we are unable to offer further insights at present with respect to the origin of the globular spongy fabric (Fig. 8E; Section 5.4) at Mangatete, a search of modern acid-dominated geothermal areas at Rotokawa and Tikitere revealed convincing modern analogs for the scalloped (compare Figs. 8F to 9H) and arcuate wavy layered (compare Figs. 8G to 9I) fabrics preserved at Mangatete. The close spatial affiliation of all four new fabrics within the North Quarry, and their inferred mixed acid-sulfate-chloride and/or fumarolic association, suggest a drop in the water table and introduction of acidic conditions at this location (cf. Jones and Renaut, 2012; discussed further in Section 7.2). This event also may have caused acid alteration overprinting of previously formed alkali chloride sinters (~36 kyr old; Section 5.3; Fig. 8A–C), and local formation of kaolin.

7.2. History of the Mangatete paleo-hydrothermal system

Prior to onset of surface paleo-hot spring activity at Mangatete, an extensive Quaternary lake system formed a catchment for airfall pyroclastics (Brathwaite, 2003). Following the period marked by the disconformity atop the lacustrine-reworked volcaniclastics, the overlying Mangatete hydrothermal system was subaerially active from at least 36 ka, and was punctuated by two hydrothermal eruption events of unknown age. Scattered, North Quarry sinter float blocks represent the earliest activity (~36 ka). These sinters were hydrothermally altered and then dismembered (Section 5.3), possibly in association with the Northern HEB event (Section 5.1). Unusual, inferred acid sinter textures also are located in the North Quarry area, thus implying a drop in the local water table (Sections 5.4, 7.1). Traces of kaolin, wüstite, and hematite were found in these sinters, which are known to be products of alteration by steam condensates (e.g., Browne, 1978). Close spatial and temporal association of neutral/alkaline springs with acid springs has been reported from other geothermal settings, such as at the margin of Lake Roto-a-Tamaheke, TVZ (Jones and Renaut, 2012).

Beginning around 22 ka, alkali chloride waters again deposited sinter in areas now positioned on both the highest (T1) and lowest (T4) of the fault terraces (Fig. 3A), with at least 45 m of vertical separation between them today. The silicified Southern HEB (Section 5.1) on T1 may delineate the throat of a paleo-vent that emitted geothermal fluids discharging toward the NW, along a lineament-controlled watercourse fed, in part, by hot springs. Both the thermal stream-derived packed fragmental sinter (PFS) and a plant-rich distal apron terrace

(Sections 5.2, 7.1) may have developed in the Deep South area (T4) in relation to this discharge (Fig. 3A). The Late Jurassic La Marciana sinter in Patagonia, Argentina, also was interpreted to have been sourced from a vent area affiliated with a hydrothermal breccia in an overall fluvial setting. While the interpreted paleo-hydrologic flow direction at Mangatete (T1 HEB to T4 Deep South sinter) may have been fault-controlled ~21 ka, the possibility of later topographic inversion and differential exhumation of indurated sinter in the study area (cf. Campbell et al., 2001, 2004) cannot be discounted. Therefore, use of present-day elevations of hydrothermal deposits to infer aspects of their history must be applied with caution.

After a ~11 kyr gap in the record of hydrothermal activity (Sections 6 and 7.3), alkali chloride waters again discharged in the Mangatete area. Dated sinter samples indicate geothermal activity at ~9.4, 6.3, 3.7 and 3.1 ka (Table 1, Fig. 3A). In particular in the South Quarry area, groundwater within the underlying lacustrine strata was heated by conduction, which extensively altered the pyroclastics to generate zeolites (mordenite, clinoptilolite) and diatomites with a cristobalite matrix (Brathwaite, 2003). This rock assemblage indicates alteration by fluids <110 °C at shallow subsurface depths of 25 to <100 m, most likely by the same fluids that the fed surface thermal spring discharges ~9.4 ka, now exposed as PFS above the present quarry level (Fig. 3A; Brathwaite, 2003). Neither the South Quarry PFS nor the other younger sinters sampled throughout the study area display features of acid-sulfate hydrothermal alteration (Section 5.2). In other words, there is no indication of extended exposure to acid steam condensate during this youngest interval (~9.4–3.1 ka) of paleo-geothermal manifestations. Thus, the history of surface hydrothermal activity at Mangatete was dynamic, and geothermal fluid compositions alternated from alkali chloride to acidic to alkali chloride conditions.

Several models (Bibby et al., 1995; Kissling and Weir, 2005; Dempsey et al., 2011; Dempsey, 2012; Rowland and Simmons, 2012) imply that the heat sources for geothermal systems in the TVZ remain stable over tens of thousands of years. However, as demonstrated herein, their surface expression varies over much shorter periods in response to events such as changes in shallow subsurface plumbing, distribution of porous host lithologies, variations in rainfall, or hydrothermal eruptions that affect the position of the piezometric surface. At Mangatete, geothermal activity lasted at least 20 kyr, but also had periods of quiescence. Ash with charcoal and charred wood at the base of a debris flow records hot temperatures locally, likely affiliated with the Taupo eruption event (~1.7 ka). The debris flow redistributed once more extensive, young (6.3–3.1 kyr old) sinter throughout the western portion of the field area.

7.3. The Mangatete paleo-hydrothermal system in relation to local tectonism

Because exposures of *in situ* sinter are discontinuous at Mangatete, any interpretation in relation to present-day spatial and temporal distribution of paleo-thermal features must be viewed with caution. Bearing this in mind, a relationship between tectonism and hydrothermal fluid flow (Fig. 10) may be speculated based on a comparison of sinter ages and their current geographic distributions in relation to timing of fault rupture through to the surface, as deduced by local paleo-seismic analysis (Canora-Catalán et al., 2008). Post-22 ka in the study area, the west strand of the Whirinaki Fault ruptured through to the surface at least five times (F1–F5 of Canora-Catalán et al., 2008; Fig. 10), incrementally increasing the elevation difference between T1 and T3 by at least 45 m. According to Canora-Catalán et al. (2008), the oldest (F5) fault rupture exposed in the Fitzpatrick trench took place sometime between ca. 21.8 ka and 15.4 ka, somewhat overlapping with the 22.7–20.7 ka sinter age grouping (S5–S7) of our study and Okareka tephra (22.1 ka) deposition. Thus the F5 event, associated with a poorly constrained dip-slip displacement of ca. 0.7 ± 0.6 m, may have been affiliated with a

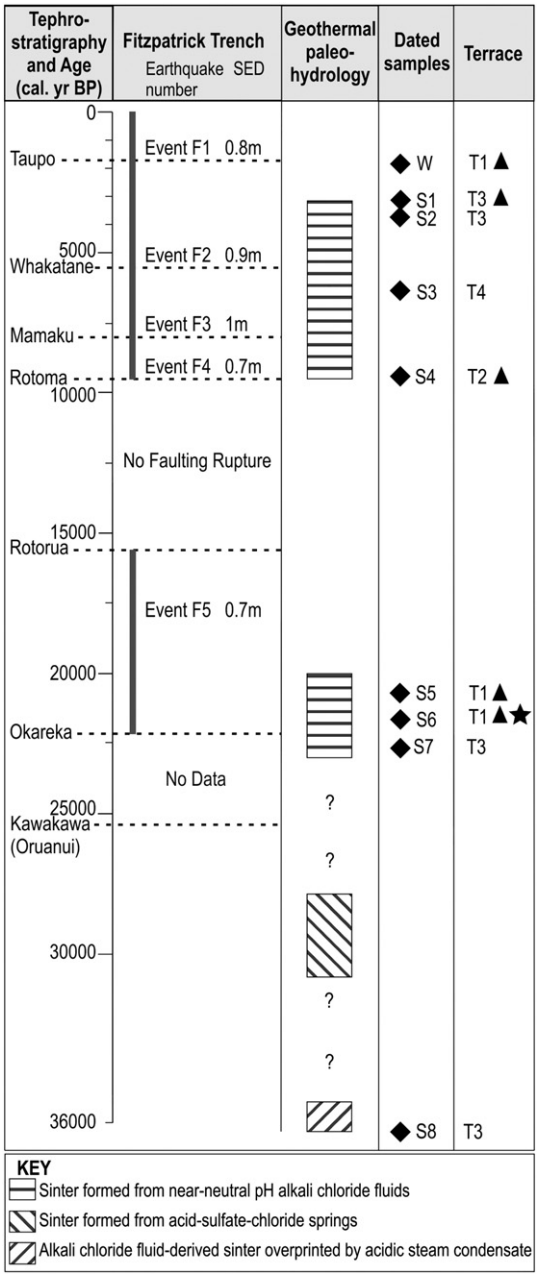

Fig. 10. Temporal correlation of paleo-seismic and paleo-hydrothermal activity at Mangatete. Radiocarbon ages of tephras identified from TVZ eruptions are indicated in relation to fault ruptures (relative timing indicated by thin gray vertical bars) derived from study of the Fitzpatrick Trench (Fig. 3A) on the west strand of the Whirinaki Fault, with the estimated amount of single-event (dip-slip) displacement (SED, in m) shown for each event (adapted from Canora-Catalán et al., 2008). Dated carbon-bearing samples from Mangatete include charred wood (W) and plant-rich sinter (S), in relation to their position on fault-controlled terraces (T1–T4) (Table 1). Triangles mark *in situ* sinter samples. Star symbol indicates that sample S6 is located on T4, but that the fluid was potentially sourced from T1 (see Fig. 3; discussed in Section 5). The paleo-hydrology column indicates temporal and compositional variation in geothermal fluids (liquid, vapor), i.e., representing alkali chloride (now acid-overprinted) to acid-sulfate-chloride to alkali chloride derived fluid discharge intervals. Relevant tephra layers (Canora-Catalán et al., 2008) are labeled with radiocarbon dates reported in Vandergoes et al. (2013) for Kawakawa/Oruanui, and from Lowe et al. (2013) for the other tephras. The reported conventional radiocarbon dates of the tephras have been calibrated herein (cf. Section 3), and presented here as mean ages with 2 sigma (95%) confidence limits, as follows: Kawakawa/Oruanui, 25,360 ± 160 cal yr BP; Okareka, 22,145 ± 117 cal yr BP; Rotorua, 15,604 ± 126 cal yr BP; Rotoma, 9502 ± 16 cal yr BP; Mamaku, 8016 ± 42 cal yr BP; Whakatane, 5542 ± 48 cal yr BP; Taupo, 1710 ± 10 cal yr BP.

volcanically active period accompanied by paleo-geothermal activity. More than 6000 years of tectonic quiescence on this strand of the Whirinaki Fault followed until a similar scale rupture occurred at 9.5 ka (F4 event; Canora-Catalán et al., 2008), contemporaneous with rhyolitic volcanism in the Okataina Volcanic Center (Fig. 1; Leonard et al., 2010; Rotoma tephra). Hydrothermal discharge at Mangatete, perhaps renewed, followed the F4 rupture event and is recorded by the presence of a ~9.4 kyr old sinter on T2. Sometime between 9.4 ka and 6.3 ka, the F3 event occurred and elevated the footwall, in a relative sense, another 0.9 ± 0.6 m. Hydrothermal discharge after this F3 event appears to have been limited to the T3 terrace.

It is unknown whether the parallel fault strands mapped in the study area were active during movements on the West Whirinaki Fault. Certainly the east strand of the Whirinaki Fault experienced two large dip-slip displacement ruptures (4.0 m ± 0.1 between 25.3 and 22.1 ka; and 2.0 ± 0.1 m between 15.6 and 9.5 ka; Canora-Catalán et al., 2008). Combining data from both the west and east fault strands, Canora-Catalán et al. (2008) determined a 0.3 ± 0.1 mm/yr dip-slip displacement rate across the Whirinaki Fault Zone for the period from 25.3 to 2 ka. Thus, elevation changes associated with regional tectonism at that time were small but nonetheless may have been sufficient to uplift shallow parts of the thermal system above the paleo-water table, resulting in a westward migration of the now-extinct, Mangatete area hot springs.

7.4. Regional paleo-hydrothermal activity in relation to TVZ structure and magmatism

The Ngakuru tectonic segment (Fig. 1) today is a thermally inactive area. However, normal faults of the Taupo Fault Belt (TFB) presently allow meteoric waters to recharge regional circulation systems. The paleo-geothermal system at Mangatete, together with other fossil surface expressions of hydrothermal activity preserved in the greater Ngakuru Graben (Fig. 2), contrast with the current inactivity. Sinters and hydrothermal eruption breccias extend NE of Mangatete for ~5 km, and some 7 km to the NW another zone of paleo-hydrothermal activity extends from Parsons Road through to the Tahunaatara sinter (Campbell et al., 2004) and to Waikaukau (Fig. 2). These sub-parallel zones, following the regional trend of the TVZ, preserve a record of thermal activity from at least 60 ka to 3 ka. In places, orthogonal, NW–SE trending lineaments suggest cross-faulting to great depths in the graywacke basement, potentially creating pipe-like conduits in the otherwise impermeable host rocks (Rowland and Sibson, 2004). Hence, a hydrothermal system may have been present at Mangatete because of enhanced permeability in a cross-fault zone. This situation is evident in the Te Kopia geothermal area, 10 km to the SSE (Bignall and Browne, 1994), and also in the Late Jurassic Deseado Massif epithermal district in Argentina (Guido and Campbell, 2011). Even allowing for quiescent periods, heat flow was probably high at Mangatete for at least 30 kyr.

Evidence for past hydrothermal eruptions in the greater Ngakuru Graben area (Fig. 2) includes not only the inferred HEBs at Mangatete but also other HEBs located 900 m to the south and 1200 m to the southeast of the North Quarry. Other local HEBs are associated with large rhyolitic boulders preserving slickensides at two sites, one oriented parallel to the Whirinaki Fault, and another 700 m to the east of T1. Two additional HEBs occur on Hossack Road, and on Corbett Road (at 1700 m and 3800 m NE of the North Quarry, respectively), and between them is the Otamakakore sinter (Holland, 2000) estimated to be ~60–120 kyr old. A parallel suite of paleo-hydrothermal activity is evident ~8 km to the northwest of Mangatete, from Parsons Road to Waikaukau (Fig. 2). Collectively these deposits follow the trend of the TFB, and suggest that they may be associated with a common regional structural weakness.

8. Conclusions

The wider Ngakuru Graben underwent significant hydrothermal activity from at least 60 ka and, at Mangatete, from ~36 ka to 3 ka. There are no proximal (i.e., very high temperature) sinters evident at Mangatete, probably owing to erosion along active faults. The North Quarry (T3) exposes *ex situ* alkali chloride sinter with typical microbial and plant fossils as old as ~36 kyr. A fall in the phreatic water level resulted in subsequent acid steam condensate overprinting of the sinter and then its dismemberment, possibly in the inferred northern HEB event. Unusual siliceous textures—vuggy, globular sponge, scalloped, arcuate wavy layered—also localized as float blocks in the North Quarry area, are inferred as acid spring sinters formed in relation to the local change in paleo-hydrology of the system. A subsequent interval of alkali chloride spring discharge (~23–21 ka) is broadly associated with West Whirinaki Fault movement (~21.8–15.4 ka) and the Okareka tephra event (~22.1 ka). The silicified Southern HEB, positioned on T1, may mark the location of paleo-thermal upflow of unknown age, along which a fault-controlled, hot spring/hot water creek may have flowed to the NW to form the Deep South Sinter on lower T4. There is a notable lack of evidence for thermal spring activity in the interval between the Rotorua and Rotoma eruptions (duration of ~6.1 kyr), during which time there was no recorded movement on the Mangatete section of the Whirinaki Fault. Following the Rotoma tephra event (~9.5 ka), alkali chloride spring deposits (≤9.4 kyr old) reappear in the stratigraphy (T2–T4). These constitute unaltered, *ex situ* and *in situ* sinters of varied textures and mineralogical maturity. Overall, the stratigraphy, geographic positions and ages of the Mangatete sinters suggest westward movement of geothermal activity until its cessation at ~3 ka. Disruption of some of the young, hydrothermally unaltered sinter (<9.5–3 kyr old) occurred in association with the Taupo eruption event ~1.8 ka, which distributed sinter blocks in a debris flow deposit that is widespread across the field area. Mangatete and the Ngakuru Graben are currently positioned in a meteoric recharge zone, with magmatism necessary during the past ~60 kyr to provide the requisite heat to sustain paleo-hydrothermal activity in the region.

Acknowledgments

This research was funded by a scholarship from Mighty River Power to BDD, and a New Zealand government MSI grant to JVR on geothermal resources of New Zealand. Field reconnaissance funds for this study were provided to KAC and PRLB from the Royal Society of New Zealand Marsden Fund. Kind advice and assistance were provided by Paul Augustinus, Bob Brathwaite, Philippa Black, Drew Downs, and David Dempsey. Steadfast support throughout the research was provided by Joy Drake. Landowners Alan Baird and Rob and Sandy van der Heuval generously allowed access to their farms. Technical assistance was supplied by Andrés Arcila, Ritchie Sims, John Wilmshurst, Catherine Hobbis and Louise Cotterall. Photography at Hot Water Creek was expertly furnished by James Reilly. Helpful reviews by Fabian Sepulveda and Rina Herdianita improved the quality of the manuscript and are gratefully acknowledged.

References

Bertrand, E.A., Caldwell, T.G., Hill, G.J., Wallin, E.L., Bennie, S.L., Cozens, N., Onacha, S.A., Ryan, G.A., Walter, C., Zaino, A., Wameyo, P., 2012. Magnetotelluric imaging of upper-crustal convection plumes beneath the Taupo Volcanic Zone, New Zealand. Geophys. Res. Lett. 39, L02304. http://dx.doi.org/10.1029/2011GL050177.

Bibby, H.M., Caldwell, T.G., Davey, F.J., Webb, T.H., 1995. Geophysical evidence on the structure of the Taupo Volcanic Zone and its hydrothermal circulation. J. Volcanol. Geotherm. Res. 68, 29–58.

Bignall, G., Browne, P.R.L., 1994. Surface hydrothermal alteration and evolution of the Te Kopia thermal area, New Zealand. Geothermics 23, 645–658.

Blank, C.E., Cady, S.L., Pace, N.R., 2002. Microbial composition of near-boiling silica-depositing thermal springs throughout Yellowstone National Park. Appl. Environ. Microbiol. 68, 5122–5135.

Boseley, C., Cumming, W., Urzúa-Monsalve, L., Powell, T., Grant, M., 2010. A resource conceptual model for the Ngatamariki geothermal field based on recent exploration well drilling and 3D MT resistivity imaging. Proceedings, World Geothermal Congress 2010, Bali, Indonesia, 25-29 April 2010.
Brathwaite, R.L., 2003. Geological and mineralogical characterization of zeolites in lacustrine tuffs, Ngakuru, Taupo Volcanic Zone, New Zealand. Clay Clay Miner. 51, 589–598.
Browne, P.R.L., 1978. Hydrothermal alteration in active geothermal fields. Annu. Rev. Earth Planet. Sci. 6, 229–250.
Browne, P.R.L., Lawless, J.V., 2001. Characteristics of hydrothermal eruptions, with examples from New Zealand and elsewhere. Earth Sci. Rev. 52, 299–331.
Bryan, C.J., Sherburn, S., Bibby, H.M., Bannister, S.C., Hurst, A.W., 1999. Shallow seismicity of the central Taupo Volcanic Zone, New Zealand: its distribution and nature. N. Z. J. Geol. Geophys. 42, 533–542.
Buddle, T.F., 2002. Sedimentary Facies and Mineralogy of the Upper Pleistocene Tahunaatara Sinter and Associated Deposits, Unpublished MSc Thesis, The University of Auckland, 152 pp., 3 appendices.
Cady, S.L., Farmer, J.D., 1996. Fossilization processes in siliceous thermal springs: trends in preservation along thermal gradients. In: Brock, G.R., Goode, J.A. (Eds.), Evolution of Hydrothermal Ecosystems on Earth (and Mars?): Ciba Foundation, 202. J. Wiley, Chichester, pp. 150–170.
Campbell, K.A., Lynne, B.Y., 2006. Diagenesis and dissolution at Sinter Island (456 yrs BP), Taupo Volcanic Zone: silica stars and the birth of quartz. Proceedings of the 28th New Zealand Geothermal Workshop (7 pp.).
Campbell, K.A., Sannazzaro, K., Rodgers, K.A., Herdianita, N.R., Browne, P.R.L., 2001. Sedimentary facies and mineralogy of the Late Pleistocene Umukuri silica sinter, Taupo Volcanic Zone, New Zealand. J. Sediment. Res. 71, 727–746.
Campbell, K.A., Buddle, T.F., Browne, P.R.L., 2004. Late Pleistocene siliceous sinter associated with fluvial, lacustrine, volcaniclastic and landslide deposits at Tahunaatara, Taupo Volcanic Zone, New Zealand. Trans. R. Soc. Edinb. Earth Sci. 94, 485–501.
Canora-Catalán, C., Villamor, P., Berryman, K., Martínez-Díaz, J.J., Raen, T., 2008. Rupture history of the Whirinaki Fault, an active normal fault in the Taupo Rift, New Zealand. N. Z. J. Geol. Geophys. 51, 277–293.
Channing, A., Edwards, D., 2009. Silicification of higher plants in geothermally influenced wetlands: Yellowstone as a Lower Devonian Rhynie analog. Palaios 24, 505–521.
Channing, A., Edwards, D., Sturtevant, S., 2004. A geothermally influenced wetland containing unconsolidated geochemical sediments. Can. J. Earth Sci. 41, 809–827.
Darby, D.J., Meertens, C.M., 1995. Terrestrial and GPS measurements of deformation across the Taupo back-arc and Hikurangi forearc regions in New Zealand. J. Geophys. Res. 100, 8221–8232.
Dempsey, D.E., 2012. Numerical Models of Tectonism and Geothermal Circulation with Application to the Taupo Volcanic Zone, New Zealand, Unpublished PhD Thesis, The University of Auckland, 278 pp.
Dempsey, D., Rowland, J., Archer, R., Ellis, S., 2011. Modelling geothermal circulation in a "TVZ-like" setting. New Zealand Geothermal Workshop, Auckland, New Zealand.
Downs, D.T., Rowland, J.V., Wilson, C.J.N., Rosenberg, M.D., Leonard, G.S., Calvert, A.T., 2014a. Evolution of the intra-arc Taupo-Reporoa Basin within the Taupo Volcanic Zone of New Zealand. Geosphere 10, 185–206.
Downs, D.T., Wilson, C.N.J., Cole, J.W., Rowland, J.V., Calvert, T.A., Leonard, G.S., 2014b. Age and eruptive center of the Paeroa Subgroup ignimbrites (Whakamaru Group) within the Taupo Volcanic Zone of New Zealand. Geol. Soc. Am. Bull. http://dx.doi.org/10.1130/B3089.1.1.
Ellis, A.J., Wilson, S.H., 1961. Hot spring areas with acid-sulphate-chloride waters. Nature 191, 696–698.
Farmer, J.D., 2000. Hydrothermal systems: doorways to early biosphere evolution. GSA Today 10, 1–9.
Farmer, J.D., Des Marais, D., 1999. Exploring for a record of ancient Martian life. J. Geophys. Res. 104 (E11), 26,977–926,995.
Fournier, R.O., Rowe, J.J., 1965. The deposition of silica in hot springs. Bull. Volcanol. 29, 585–587.
Giggenbach, W.F., 1984. Mass transfer in hydrothermal alteration systems–a conceptual approach. Geochim. Cosmochim. Acta 48, 2693–2711.
Gravley, D.M., Wilson, C.J.N., Rosenberg, M.D., Leonard, G.S., 2006. The nature and age of Ohakuri Formation and Ohakuri Group rocks in surface exposures and geothermal drillhole sequences in the central Taupo Volcanic Zone, New Zealand. N. Z. J. Geol. Geophys. 49, 305–308.
Grindley, G.W., 1959. Geological Map NZ 1:63360, Sheet 8, Waiotapu. DSIR, Wellington, NZ.
Guido, D.M., Campbell, K.A., 2011. Jurassic hot spring deposits of the Deseado Massif (Patagonia, Argentina): characteristics and controls on regional distribution. J. Volcanol. Geotherm. Res. 203, 35–47.
Guido, D.M., Channing, A., Campbell, K.A., Zamuner, A., 2010. Jurassic geothermal landscapes and ecosystems at San Agustín, Patagonia, Argentina. J. Geol. Soc. Lond. 167, 11–20.
Guidry, S.A., Chafetz, H.S., 2003a. Anatomy of siliceous hot spring examples from Yellowstone National Park, Wyoming, U.S.A. Sediment. Geol. 157, 71–106.
Guidry, S.A., Chafetz, H.S., 2003b. Depositional facies and diagenetic alteration in a relict siliceous hot-spring accumulation: examples from Yellowstone National Park, U.S.A. J. Sediment. Res. 73, 806–823.
Handley, K.M., Campbell, K.A., 2011. Character, analysis and preservation of biogenicity in terrestrial siliceous stromatolites from geothermal settings. In: Tewari, V.C., Seckbach, J. (Eds.), Stromatolites: Interaction of Microbes with Sediments. Springer, pp. 359–381.
Hedenquist, J.W., 1986. Geothermal systems in the Taupo Volcanic Zone: their characteristics and relation to volcanism and mineralization. In: Smith, I.E.M. (Ed.), Late Cenozoic Volcanism in New Zealand. Royal Society of New Zealand Bulletin, 23, pp. 134–168.
Hedenquist, J.W., Browne, P.R.L., 1989. The evolution of the Waiotapu geothermal system, New Zealand, based on the chemical and isotopic composition of its fluids, minerals and rocks. Geochim. Cosmochim. Acta 53, 2235–2257.
Herdianita, N.R., Rodgers, K.A., Browne, P.R.L., 2000a. Routine instrumental procedures to characterize the mineralogy of modern and ancient silica sinters. Geothermics 29, 65–81.
Herdianita, N.R., Browne, P.R.L., Rodgers, K.A., Campbell, K.A., 2000b. Mineralogical and textural changes accompanying ageing of silica sinter. Mineral. Deposita 35, 48–62.
Hinman, N.W., Lindstrom, R.F., 1996. Seasonal changes in silica deposition in hot spring systems. Chem. Geol. 132, 237–246.
Hochstein, M.P., 1995. Crustal heat transfer in the Taupo Volcanic Zone (New Zealand): comparison with other volcanic arcs and explanatory heat source models. J. Volcanol. Geotherm. Res. 68, 117–151.
Hogg, A., Hua, Q., Blackwell, P.G., Niu, M., Buck, C.E., Guilderson, T.P., Heaton, T.J., Palmer, J.G., Reimer, P.J., Reimer, R.W., Turney, C.S.M., Zimmerman, S.R.H., 2013. SHCal13 Southern Hemisphere calibration, 0–50,000 years cal BP. Radiocarbon 55, 1889–1903.
Holland, G.R., 2000. The Whirinaki Sinter, Taupo Volcanic Zone, Unpublished MSc Thesis, The University of Auckland, 114 pp., 1 appendix.
Houghton, B.F., Wilson, C.J.N., McWilliams, M.O., Lanphere, M.A., Weaver, S.D., Briggs, R. M., Pringle, M.S., 1995. Chronology and dynamics of a large silicic magmatic system: central Taupo Volcanic Zone, New Zealand. Geology 23, 13–16.
Jones, B., Renaut, R.W., 2003. Hot spring and geyser sinters: the integrated product of precipitation replacement, and deposition. Can. J. Earth Sci. 40, 1549–1569.
Jones, B., Renaut, R.W., 2007. Microstructural changes accompanying the opal-A to opal-CT transition: new evidence from the siliceous sinters of Geysir, Haukadalur, Iceland. Sedimentology 54, 921–948.
Jones, B., Renaut, R.W., 2012. Facies architecture in depositional systems resulting from the interaction of acidic springs, alkaline springs, and acidic lakes: case study of Lake Roto-a-Tamaheke, Rotorua, New Zealand. Can. J. Earth Sci. 49, 1217–1250.
Jones, B., Renaut, R.W., Rosen, M.R., 1997. Biogenecity of silica precipitation around geysers and hot-spring vents, North Island, New Zealand. J. Sediment. Res. 67, 88–104.
Jones, B., Renaut, R.W., Rosen, M.R., 1998. Microbial biofacies in hot-spring sinters: a model based on Ohaki Pool, North Island, New Zealand. J. Sediment. Res. 68, 413–434.
Jones, B., Renaut, R.W., Rosen, M.R., 1999a. Role of fungi in the formation of siliceous coated grains, Waiotapu geothermal area, North Island, New Zealand. Palaios 14, 475–492.
Jones, B., Renaut, R.W., Rosen, M.R., 1999b. Actively growing siliceous oncoids in the Waiotapu geothermal area, North Island, New Zealand. J. Geol. Soc. Lond. 156, 89–103.
Jones, B., Renaut, R.W., Rosen, M.R., 2000. Stromatolites forming in acidic hot-spring waters, North Island, New Zealand. Palaios 15, 450–475.
Jones, B., Renaut, R.W., Rosen, M.R., 2001. Taphonomy of silicified filamentous microbes in modern geothermal sinters - implications for identification. Palaios 16, 580–592.
Jones, B., Renaut, R.W., Rosen, M.R., 2003. Silicified microbes in a geyser mound: the enigma of low-temperature cyanobacteria in a high-temperature setting. Palaios 18, 87–109.
Jones, B., Renaut, R.W., Konhauser, K.O., 2005. Genesis of large siliceous stromatolites at Frying Pan Lake, Waimangu geothermal field, North Island, New Zealand. Sedimentology 52, 1229–1252.
Kissling, W.M., Weir, G.J., 2005. The spatial distribution of the geothermal fields in the Taupo Volcanic Zone, New Zealand. J. Volcanol. Geotherm. Res. 145, 136–150.
Konhauser, K.O., Jones, B., Reysenbach, A.-L., Renaut, R.W., 2003. Hot spring sinters: keys to understanding Earth's earliest life forms. Can. J. Earth Sci. 40, 1713–1724.
Krupp, R.E., Seward, T.M., 1987. The Rotokawa geothermal system, New Zealand. Econ. Geol. 82, 1109–1129.
Leonard, G.S., Begg, J.G., Wilson, C.J.N., 2010. Geology of the Rotorua Area. Institute of Geological and Nuclear Sciences, Lower Hutt, New Zealand (102 pp. + Map).
Letelier, P.A., 2004. The Natural Thermal Features at the Tikitere Geothermal Field and the Characteristics of its Surface Deposits, unpublished MSc Thesis, The University of Auckland, 121 pp.
Lowe, D.R., Braunstein, D., 2003. Microstructure of high-temperature (>73 °C) siliceous sinter deposited around hot springs and geysers, Yellowstone National Park: the role of biological and abiological processes in sedimentation. Can. J. Earth Sci. 40, 1611–1642.
Lowe, D.R., Anderson, K.S., Braunstein, D., 2001. The zonation and structuring of siliceous sinter around hot springs, Yellowstone National Park, and the role of thermophilic bacteria in its deposition. In: Reyensbach, A.M., Voytech, M., Mancinelli, R. (Eds.), Thermophiles: Biodiversity. Ecology and Evolution. Kluwer Academic/Plenum Publishers, New York, pp. 143–166.
Lowe, D.J., Blaauw, M., Hogg, A.G., Newnham, R.M., 2013. Ages of 24 widespread tephras erupted since 30,000 years ago in New Zealand, with re-evaluation of the timing and palaeoclimatic implications of the Late Glacial cool episode recorded at Kaipo bog. Quat. Sci. Rev. 74, 170–194.
Lynne, B.Y., 2012. Mapping vent to distal-apron hot spring paleo-flow pathways using siliceous sinter architecture. Geothermics 43, 3–24.
Lynne, B.Y., Campbell, K., 2003. Diagenetic transformations (opal-A to quartz) of low- and mid-temperature microbial textures in siliceous hot-spring deposits, Taupo Volcanic Zone, New Zealand. Can. J. Earth Sci. 40, 1679–1696.
Lynne, B.Y., Campbell, K.A., 2004. Morphologic and mineralogic transitions from opal-A to opal-CT in low-temperature siliceous sinter diagenesis, Taupo Volcanic Zone, New Zealand. J. Sediment. Res. 74, 561–579.
Lynne, B.Y., Campbell, K.A., Moore, J.N., Browne, P.R.L., 2005. Diagenesis of 1900-year-old siliceous sinter (opal-A to quartz) at Opal Mound, Roosevelt Hot Springs, Utah, U.S.A. Sediment. Geol. 179, 249–278.
Lynne, B.Y., Campbell, K.A., Perry, R.S., Browne, P.R.L., Moore, J.N., 2006. Acceleration of sinter diagenesis in an active fumarole, Taupo volcanic zone, New Zealand. Geology 34, 749–752.

Lynne, B.Y., Campbell, K.A., James, B.J., Browne, P.R.L., Moore, J., 2007. Tracking crystallinity in siliceous hot-spring deposits. Am. J. Sci. 307, 612–641.
Manville, V., 2001. Sedimentology and history of Lake Reporoa: an ephemeral supra-ignimbrite lake. Taupo Volcanic Zone, New Zealand. In: White, J.D.L., Riggs, N.R. (Eds.), Volcaniclastic Sedimentation in Laucustrine Settings. Blackwell Science, Malden MA, pp. 109–140.
Mountain, B.W., Benning, L.G., Boerema, J.A., 2003. Experimental studies on New Zealand hot spring sinters: rates of growth and textural development. Can. J. Earth Sci. 40, 1643–1667.
Murphy, B.A., 2013. Siliceous Hotspring (Sinter) Deposits along the Paeroa Fault (TVZ): Archives of Geothermal Fluid History. Unpublished MSc Thesis, The University of Auckland, 163 pp.
Nairn, I.A., 2002. Geology of the Okataina Volcanic Centre, scale 1:50,000. Institute of Geological & Nuclear Sciences Geological Map 25. Lower Hutt, New Zealand: Institute of Geological & Nuclear Sciences Ltd., 1 sheet + 156 pp.
Pentecost, A., 2003. Cyanobacteria associated with hot spring travertines. Can. J. Earth Sci. 40, 1447–1457.
Renaut, R.W., Jones, B., 2011. Hydrothermal environments, terrestrial. In: Reitner, J., Thiel, V. (Eds.), Encyclopedia of Geobiology. Springer, pp. 467–479.
Rodgers, K.A., Cook, K.L., Browne, P.R.L., Campbell, K.A., 2002. The mineralogy, texture and significance of silica derived from alteration by steam condensate in three New Zealand geothermal fields. Clay Miner. 37, 299–322.
Rodgers, K.A., Browne, P.R.L., Buddle, T.F., Cook, K.L., Greatrex, R.A., Hampton, W.A., Herdianita, N.R., Holland, G.R., Lynne, B.Y., Martin, R., Newton, Z., Pastars, D., Sannazarro, K.L., Teece, C.I.A., 2004. Silica phases in sinters and residues from geothermal fields of New Zealand. Earth Sci. Rev. 66, 1–61.
Rowland, J.V., Sibson, R.H., 2001. Extensional fault kinematics within the Taupo Volcanic Zone, New Zealand: soft-linked segmentation of a continental rift system. N. Z. J. Geol. Geophys. 44, 271–283.
Rowland, J.V., Sibson, R.H., 2004. Structural controls on hydrothermal flow in a segmented rift system, Taupo Volcanic Zone, New Zealand. Geofluids 4, 259–283.
Rowland, J.V., Simmons, S.F., 2012. Hydrologic, magmatic, and tectonic controls on hydrothermal flow, Taupo Volcanic Zone, New Zealand: implications for the formation of epithermal vein deposits. Econ. Geol. 107, 427–457.
Rowland, J.V., Wilson, C.J.N., Gravley, D.M., 2010. Spatial and temporal variations in magma-assisted rifting, Taupo Volcanic Zone, New Zealand. J. Volcanol. Geotherm. Res. 190, 89–108.
Ruff, S.W., Farmer, J.D., Calvin, W.M., Herkenhoff, K.E., Johnson, J.R., Morris, R.V., Rice, M.S., Arvidson, R.E., Bell III, J.F., Christensen, P.R., Squyres, S.W., 2011. Characteristics, distribution, origin and significance of opaline silica observed by Spirit rover in Gusev crater, Mars. J. Geophys. Res. 116, E00F23.
Schinteie, R., Campbell, K.A., Browne, P.R.L., 2007. Microfacies of stromatolitic sinter from acid-sulphate-chloride springs at Parariki stream, Rotokawa Geothermal Field, New Zealand. Palaeontol. Electron. 10 (1; 4A), 33.
Seebeck, H., Nicol, A., 2009. Dike intrusion and displacement accumulation at the intersection of the Okataina Volcanic Centre and Paeroa Fault zone, Taupo Rift, New Zealand. Tectonophysics 475, 575–585.
Sillitoe, R.H., 1993. Epithermal models: genetic types, geometrical controls and shallow features. In: Kirkham, R.V., et al. (Eds.), Mineral Deposit Modeling: Geological Association of Canada. Special Volume, 40, pp. 403–417.
Simmons, S.F., 1995. A field guide to the hydrothermal systems of the North Island, New Zealand: active and extinct epithermal environments. Pacrim '95 Congress, Auckland, Australian Institute of Mining and Metallurgy, pp. 1–12.
Stagpoole, V.M., Bibby, H.M., 1998. Electrical resistivity map of the Taupo Volcanic Zone, New Zealand; nominal array spacing 500 m, 1:250 000, version 1.0. Institute of Geological and Nuclear Sciences Geophysical Map 11. Institute of Geological and Nuclear Sciences, Lower Hutt, New Zealand.
Tewari, V., Seckbach, J. (Eds.), 2011. Stromatolites: Interaction of Microbes with Sediments. Springer, Dordrecht, Heidelberg, London, New York (751 pp.).
Tice, M.M., Thornton, D.C.O., Pope, M.C., Olszewski, T.D., Gong, J., 2011. Archaean microbial mat communities. Annu. Rev. Earth Planet. Sci. 39, 297–319.
Trewin, N.H., Fayers, S.R., Kelman, R., 2003. Subaqueous silicification of the contents of small ponds in an Early Devonian hot-spring complex, Rhynie, Scotland. Can. J. Earth Sci. 40, 1697–1712.
Vandergoes, M.J., Hogg, A.G., Lowe, D.J., Newnham, R.M., Denton, G.H., Southon, J., Barrell, D.J.A., Wilson, C.J.N., McGlone, M.S., Allan, A.S.R., Almond, P.C., Petchey, F., Dabell, K., Dieffenbacher-Krall, A.C., Blaauw, M., 2013. A revised age for the Kawakawa/Oruanui tephra, a key marker for the Last Glacial Maximum in New Zealand. Quat. Sci. Rev. 74, 195–201.
Villamor, P., Berryman, K., 2001. A late Quaternary extension rate in the Taupo Volcanic Zone, New Zealand, derived from fault slip data. N. Z. J. Geol. Geophys. 44, 243–269.
Wallace, L.M., Bevan, J., McCaffrey, R., Darby, D.J., 2004. Subduction zone coupling and tectonic block rotations in the North Island, New Zealand. J. Geophys. Res. 109 (B12406).
Walter, M.R., 1976. Hot-spring sediments in Yellowstone National Park. In: Walter, W.R. (Ed.), Stromatolites. Developments in Sedimentology. , 20. Elsevier, pp. 489–498.
Walter, M.R., Bauld, J., Brock, T.D., 1976. Microbiology and morphogenesis of columnar stromatolites (*Conophyton*, *Vacerrilla*) from hot springs in Yellowstone National Park. In: Walter, W.R. (Ed.), Stromatolites. Developments in Sedimentology. 20. Elsevier, pp. 273–310.
Walter, M.R., Des Marais, D., Farmer, J.D., Hinman, N.W., 1996. Lithofacies and biofacies of mid-Paleozoic thermal spring deposits in the Drummond Basin, Queensland, Australia. Palaios 11, 497–518.
Wan, T., Hedenquist, J.W., 1981. A reassessment of the structural control of the Broadlands geothermal field, New Zealand. Proceedings of the 3rd New Zealand Geothermal Workshop, Auckland, pp. 195–202.
White, D.E., Brannock, W.W., Murata, K.J., 1956. Silica in hot springs. Geochim. Cosmochim. Acta 10, 27–57.
White, D.E., Thompson, G.A., Sandberg, C.H., 1964. Rocks, structure, and geologic history of Steamboat Springs thermal area, Washoe County, Nevada. U.S. Geological Survey Professional Paper. 458-B (63 pp.).
Wilson, C.J.N., Houghton, B.F., McWilliams, M.O., Lamphre, M.A., Weaver, S.D., Briggs, R.M., 1995. Volcanic and structural evolution of Taupo Volcanic Zone, New Zealand: a review. J. Volcanol. Geotherm. Res. 68, 1–28.